Biocompuesto de matriz celulósica y puntos cuánticos de carbono para la detección de mercurio en efluentes acuosos

Laura Andrea Rojas Palomino
Química Ambiental

Universidad Industrial de Santander

Facultad de Ciencias, Escuela de Química

Maestría en Química

Bucaramanga

2025

Biocompuesto de matriz celulósica y puntos cuánticos de carbono para la detección de mercurio en efluentes acuosos

Laura Andrea Rojas Palomino
Química Ambiental

Tesis presentada para optar al título de magister en química

Directora:
Marianny Yajaira Combariza Montañez
Química, PhD

Codirector:
Carlos Andrés Martínez Bonilla
Químico, MSc en Ingeniería de materiales

Universidad Industrial de Santander
Facultad de Ciencias, Escuela de Química
Maestría en Química
Bucaramanga
2025

Acknowledgment

To my advisor, Dr. Marianny Yajaira Combariza Montañez, for the invaluable support provided during the execution of this research project and for the knowledge imparted throughout this process.

To my co-advisor, Carlos Andrés Martínez Bonilla, for the unwavering support offered during this research, and for the knowledge and guidance shared along the way.

To the evaluators, for their valuable contributions and suggestions during the assessment of this research work.

To the Industrial University of Santander, for welcoming me into its community and allowing me to pursue graduate studies at its esteemed institution.

To the faculty of the Chemistry Department for their exceptional teaching and for their significant contribution to my professional development.

To the Center for Environmental Studies and Research (CEIAM) at the Industrial University of Santander.

To the Research Group on Theoretical and Experimental Physical Chemistry (GIFTEX) at the Industrial University of Santander.

To the SENUMA research group at the Santo Tomás University, Bucaramanga section.

To project 844/2019 COD 121384468197, Contract 770-2020, funded by Minciencias.

To project BPIN 2020000100258, financed by the General Royalties System and executed by the Industrial University of Santander.

To my family for their unconditional support, patience, and love throughout this journey. Their faith in me was instrumental in achieving this milestone.

To my friends and colleagues, Claudia Cajicá, Evelyn Calderón, Laura Pinto, Silvia Corrales, Stefany Mora, and Carlos Andrés Padilla, for their friendship, understanding. Their support was essential on this journey.

Table of contents

List of Figures

Listo f Tables

List of appendixes

Resumen

Título: Biocompuesto de matriz celulósica y puntos cuánticos de carbono para la detección de mercurio en efluentes acuosos

Autor: Laura Andrea Rojas Palomino, Química Ambiental

Palabras claves: Puntos cuánticos de carbono (CQDs), Monitoreo ambiental, Nanocelulosa, Biocomposito

Este estudio explora la influencia de las técnicas de purificación en las propiedades ópticas, la química superficial y las capacidades de detección de mercurio de los puntos cuánticos de carbono (CQDs). Se evaluaron dos métodos de purificación, diálisis (CQDs-DL) y cromatografía en columna (CQDs-CC). Los resultados demuestran diferencias significativas en la estructura de la superficie, ya que los CQDs-DL presentan más grupos NH_2, NH_3 e imina, lo que conduce a un mayor apagado de la fluorescencia en presencia de mercurio que los CQDs-CC, que presentan principalmente grupos NH_2. El sensor, fabricado a partir de CQDs, se evaluó en solución y en un biocompuesto. El comportamiento del sensor se evaluó primero en solución, comparando ambos métodos de purificación. Posteriormente, se probó su rendimiento en un biocompuesto de nanocelulosa bacteriana (CQDs/TOCN), revelando que CQDs-CC ofrece una respuesta de extinción más estable y lineal. Además, el análisis de muestras reales de fuentes de agua contaminadas con mercurio confirmó la eficacia del sensor, ya que ambos CQDs mostraron cambios de fluorescencia al interactuar con el mercurio. Estos resultados sugieren que, aunque la diálisis es un método de purificación común, puede no ser siempre óptimo, ya que la cromatografía en columna ofrece una purificación fina adecuada para aplicaciones específicas de detección medioambiental. Este trabajo pone de relieve el potencial de los sensores basados en CQD para la monitorización en tiempo real de la contaminación por metales pesados en fuentes de agua.

Abstract

Title: Biocomposite of cellulose matrix and Carbon Quantum Dots (NCB/CQDs) for detecting mercury in aqueous effluents.

Autor: Laura Andrea Rojas Palomino, Environmental Chemist.

Keywords: Carbon Quantum Dots (CQDs), Environmental Monitoring, Nanocellulose Biocomposite

This study explores the influence of purification techniques on the optical properties, surface chemistry, and sensing capabilities of carbon quantum dots (CQDs) in environmental applications, particularly for mercury detection. Two purification methods, dialysis (CQDs-DL) and column chromatography (CQDs-CC), were evaluated. The results demonstrate significant differences in the surface structure, with CQDs-DL exhibiting more NH_2, NH_3, and imine groups, leading to greater fluorescence quenching in the presence of mercury than CQDs-CC, which primarily features NH_2 groups. The sensor, made from CQDs, was evaluated in solution and a biocomposite. The sensor behavior was first assessed in solution, comparing both purification methods. Subsequently, its performance was tested in a bacterial nanocellulose biocomposite (CQDs/TOCN), revealing that CQDs-CC offers a more stable and linear quenching response. Additionally, real-sample analysis from mercury-contaminated water sources confirmed the sensor efficacy, with both CQDs showing fluorescence shifts upon interaction with mercury. These findings suggest that although dialysis is a common purification method, it may not always be optimal, as column chromatography offers fine purification suitable for specific environmental sensing applications. This work highlights the potential of CQD-based sensors for the real-time monitoring of heavy metal contamination in water sources.

Introduction

The global extent of chemical contamination in aquatic sources caused by heavy metals (HMs) in water has become a worldwide issue due to the rapid growth of industrialization, urbanization, and the use of chemical compounds across various industries (Hama Aziz et al., 2023). HMs contamination represents a primary environmental and public health concern due to its high toxicity to fauna and flora, environmental persistence, and potential bioaccumulation. These factors adversely affect the nervous systems of living organisms (Zhang et al., 2023). Furthermore, the presence of HMs in the agricultural sector results in significant losses and/or increased costs for the treatment and bioremediation of crops (Hama Aziz et al., 2023). Mercury (Hg^{2+}) is one of the most problematic HMs because of its ability to bioaccumulate and biomagnify in ecosystems, allowing it to affect biochemical and physiological processes in animals and plants rapidly(United Nations Environment Programme (UNEP), 2013).

Currently, Hg^{2+} is introduced into the ecosystem through various mechanisms, including the processing of fossil fuels, waste incineration, and mining activities (Zou et al., 2020). Colombia is no exception in this regard, as it has a high level of mining activity, characterized by artisanal and low-tech extraction processes, which result in low productivity and high contamination levels in water bodies, particularly near the Paramo regions (Rodríguez, 2019). With the increasing presence of Hg^{2+} and other HMs in rivers, real-time monitoring and control systems have been implemented. However, these systems still have deficiencies and require investment in research projects to improve and develop more straightforward, cost-effective, and faster analysis and detection technologies. This positively impacts environmental control and decision-making related to the environment (Kasinathan et al., 2022; Zou et al., 2020). Some technologies for identifying and removing HMs from freshwater bodies have been implemented, including robust analytical techniques such as atomic absorption spectroscopy (AAS) and inductively coupled plasma optical emission spectroscopy (ICP-OES) (Zhu et al., 2023). Techniques such as ion exchange, advanced oxidation, chemical precipitation, adsorption, and reverse osmosis have also been applied (Hama Aziz et al., 2023).

In recent years, research aimed at developing faster and more selective methods for identifying and quantifying HMs has intensified, with the latest advancements highlighting the use of nanomaterials as sensors (Lv et al., 2022). Due to their small size and large surface area, nanomaterials can effectively interact with metal ions, improving their sensitivity and selectivity in detecting trace amounts of HMs in various samples (Vonnie et al., 2022). Carbon Quantum Dots (CQDs) are nanomaterials that effectively detect Hg^{2+}. The response of CQDs to specific heavy metals varies according to their concentration (Zhu et al., 2023).

The CQDs have been regarded as versatile “green” compounds with a wide range of chemical applications due to their unique chemical and physical properties (Guan et al., 2023). These compounds exhibit excellent chemical and physical stability, low toxicity, good electrical conductivity, environmental compatibility, and optical properties comparable to traditional quantum dots, such as CdSe, CdTe, and gold and silver nanoparticles (García de Arquer et al., 2021). Additionally, CQDs can be produced from renewable sources such as biomass-derived materials, plant-based precursors, and agricultural waste, making these compounds an excellent option for exploring renewable technologies and applications in several fields (Meng et al., 2019).

It is essential to highlight that crude reaction mixtures of CQDs (Rxn) contain numerous emissive and non-emissive molecular by-products that are excluded during purification (Chen et al., 2019). So far, only a few separation systems have been developed for these nanomaterials, which can be classified into macro and fine categories (G. Guo & Xia, 2024). In most studies on the synthesis of CQDs, dialysis (macro separation) remains the most widely used purification method. However, no standard procedures are associated with the duration of dialysis or the choice of the molecular weight cut-off (MWCO) for the dialysis membrane (Chen et al., 2019). On the other hand, fine separation through chromatographic techniques, like column chromatography, is a separation tool that takes into account factors such as affinity, polarity, and solubility (G. Guo & Xia, 2024).

The quality of purification can affect the limit of detection (LOD) of CQDs-based sensors, influencing their specificity and sensitivity for detecting HMs at low concentrations (ppb range) (Escandar & Olivieri, 2022). Moreover, the fabrication of detection devices requires a matrix or support material that enhances the sensor's specificity, sensitivity, and overall performance. This matrix stabilizes and improves the sensor's response to target substances, ensuring reliable and accurate detection (Ma et al., 2023). Using nanocellulose (NC) as a sensor matrix is an excellent renewable option that offers properties such as biocompatibility, low toxicity, and relatively low production costs. Bacterial nanocellulose (BNC) is a highly pure form of cellulose produced by *Gluconacetobacter xylinus* as a three-dimensional network at the nanoscale. This structure provides exceptional properties that enhance sensor stability, increase the surface area for interaction with analytes, and allow for efficient signal transduction during detection applications (Reshmy et al., 2021). NC surface modification is essential for improving interactions and compatibility with other compounds. TEMPO (2,2,6,6-tetramethylpiperidine-1-oxyl) oxidation of cellulose produces TEMPO-oxidized nanocellulose with excellent colloidal stability and flexible surface chemistry. Hydro- and aerogels of cellulose nanofibers serve as scaffolds in advanced materials that require improved stability, mechanical strength, and customizable functionalization (Saavedra-Sanabria et al., 2021).

This study investigated the production of biosensors made from CQDs dispersed in an NC matrix for detecting mercury in surface water sources. CQDs were synthesized and then purified using dialysis and column chromatography. The effects of the purification techniques on the structural characteristics, optical properties, and sensing performance of CQDs were assessed. The sensitivity and specificity of CQDs-based biosensors for environmental mercury detection were affected by the CQDs purification technique.

Problem Statement

Water quality is significantly impacted by the rise of emerging contaminants, including pharmaceuticals, pesticide residues, dyes, and HMs (Kumar et al., 2022). Both natural and anthropogenic introductions of the latter have resulted in the presence of elements like mercury and cadmium, which has led to a decrease in biodiversity (Hama Aziz et al., 2023) and a significant risk of access to safe water (IDEAM (Instituto de Hidrología, 2019). This situation raises concerns because Regulation 631 of 2015, which governs the presence of HMs in Colombia's aquatic effluents, is more lenient regarding surveillance, monitoring, and control compared to international standards (Rodríguez, 2019). The latest water monitoring and follow-up protocol presented by IDEAM was in 2021, when 160 water quality monitoring points were established across the country, eight of which are in the department of Santander, with three near the municipalities of Surata, Vetas, and California. The same report included HMs sampling in water and sediments, measuring metals such as aluminum, cadmium, copper, chromium, iron, manganese, nickel, lead, mercury, and zinc at 106 monitoring stations (IDEAM, (Instituto de Hidrología, 2021).

One of the primary economic activities in the municipality of Vetas-Santander is artisanal gold mining, which involves the use of Hg^{2+} to separate gold from ore. Independent studies on water quality in Vetas have shown that Hg^{2+} concentrations exceed the limits set by Resolution 2115 of 2007, adversely affecting the health of individuals involved in this activity and threatening the municipality's water resources. (Rodríguez, 2019). In light of this, various pathways for Hg^{2+} introduction into the environment have been observed (e.g., diffusion, deposition, and suspension), as illustrated in Figure 1, along with the risks associated with small-scale mining. (United Nations Environment Programme (UNEP), 2013). Around the world, most techniques commonly used for monitoring HMs include detection and quantification away from the sampling point, which requires proper collection, storage, and pre-analysis treatment protocols. Additionally, these traditional methods have several disadvantages, including complex pretreatment processes, the need for certified standards, and the requirement for advanced equipment such as AAS and ICP-MS, among others (Zhu et al., 2023).

Figure 1. *Risks and Pathways of Mercury Introduction into the Environment, adapted from (UNEP, 2013)*

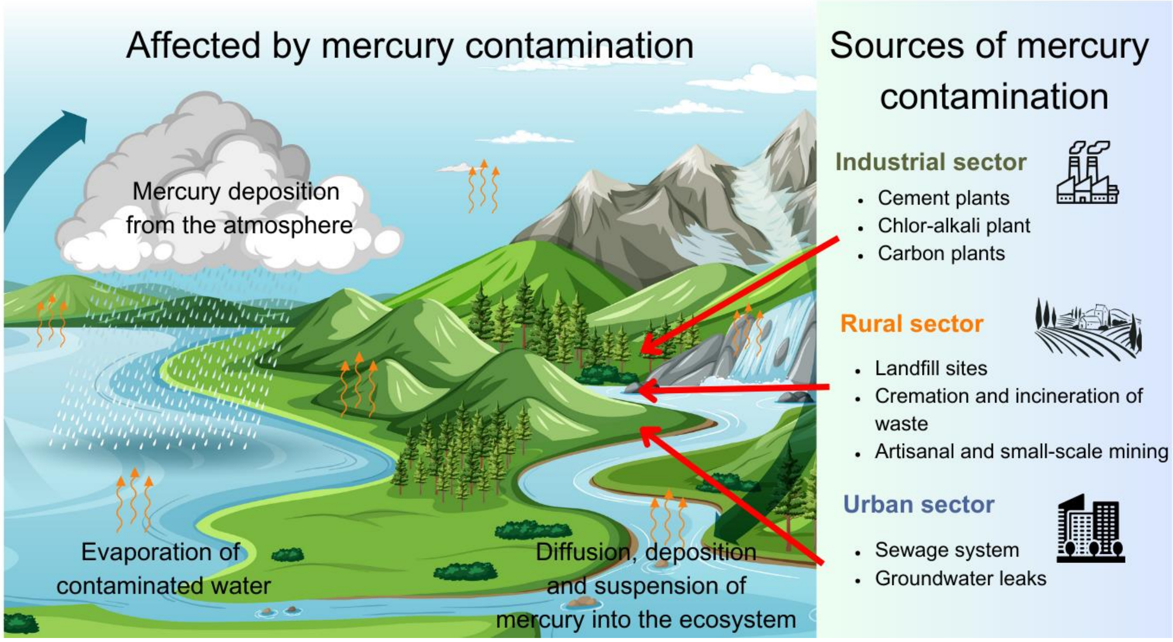

Sensors are emerging as alternatives for in-situ monitoring of HMs. New materials facilitating swift and efficient detection of contaminants, particularly CQDs, are revolutionizing the field of in-situ HMs detection. CQDs showcase a variety of optical and functional characteristics that enhance their effectiveness as detection systems. Notably, the specific color emissions from CQDs vary according to their composition, morphology, and synthesis techniques. Fluorescence assays highlight several advantages of CQDs, including exceptional sensitivity, quick analysis, and minimal adverse effects on samples, affirming their potential as a promising alternative to traditional detection methods (Zou et al., 2020). However, it is essential to emphasize that despite these properties, the use of CQDs has been limited due to the lack of control over synthesis methods and the challenges in understanding the photoluminescence mechanism and the relationship between structure and properties (Ozyurt et al., 2023). The carbonaceous materials as Carbon dots (CDs) can be classified into three categories: (1) graphene quantum dots (GQDs), (2) carbon nanodots (CNDs), and (3) polymer dots (PDs), as illustrated in Figure 2. Spherical CNDs can be divided into two subgroups: carbon nanoparticles (CNPs) and CQDs of interest, represented as multiple layers of graphene and surface chemical groups (Ozyurt et al., 2023).

The purification methods of CQDs can be categorized into coarse and fine (G. Guo & Xia, 2024). In most studies on the synthesis of CQDs, dialysis is the most popular and widely used purification method. After CQDs synthesis, the reaction solution is filtered and dialyzed using deionized water. However, there is no standard for dialysis time or for selecting the dialysis membrane's molecular weight cutoff (MWCO) (Chen et al., 2019).

Figure 2. *Classification of the different types of CDs. Adapted from (Ozyurt et al., 2023).*

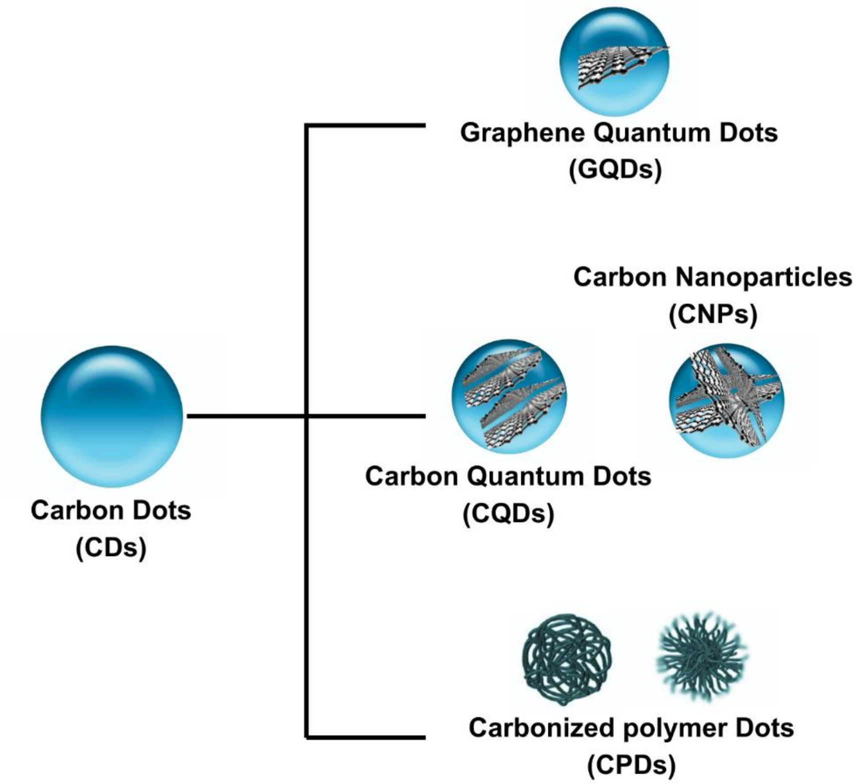

Justification

The search for alternatives in devices that allow for rapid and efficient identification and quantification of HMs for real-time environmental monitoring is one of the primary current challenges in environmental science (Vonnie et al., 2022). Colombian water resources require real-time and up-to-date monitoring of HMs to enable a quick diagnosis of pollution levels. Consequently, a device that is easy to handle and transport provides a rapid and reliable response, with a detection limit close to the maximum allowed values according to Resolution 2115 of 2007 and offers an in-situ response for the detection of HMs, could be applied to real samples and contribute to the establishment of a monitoring network.

In the last decade, the "nano-revolution" has taken center stage in the field of new materials, with nanomaterials being particularly attractive because of their unique thermal, mechanical, and optoelectronic properties. Their high surface-to-volume ratio and possibility of surface functionalization make them ideal for the fabrication of detection devices (Zhu et al., 2023). Among these nanomaterials, CQDs stand out for their optical properties, which enable the development of efficient sensors for detecting various types of ions(Zou et al., 2020). Sensors can be classified according to the stimuli they receive (Table 1). Specifically, chemical sensors are classified based on their operational principles, which allow them to detect and quantify specific chemicals in various environments. These classifications emphasize the diversity of technologies and materials used in the design of sensors to meet the requirements of different applications (Lamkin-kennard & Popovic, 2019).

***Table 1**. Quantities commonly measured by sensors based on the type of stimulus. Adapted from (Lamkin-kennard & Popovic, 2019)*

Type of stimulus	Measured
Chemical	Concentration
Electrical	Current, charge, electric field, conductivity, resistance
Optical	Absorption, reflection, refractive index
Mechanical	Displacement, velocity, acceleration, torque, stress, strain, pressure
Thermal	Temperature, specific heat, thermal flux, thermal conductivity

Unlike traditional semiconductor quantum dots, which contain HMs, CQDs are entirely composed of carbon, making them significantly safer for applications ranging from electronics to biomedicine (Arivarasan et al., 2022). Similarly, their synthesis can be achieved through relatively simple and cost-effective methods, reducing the overall production cost compared with other types of quantum dots. Despite their structural simplicity, CQDs exhibit excellent optical properties including broad absorbance and bright luminescence, which can be fine-tuned by controlling their size and surface chemistry (Ozyurt et al., 2023). The latter can be easily modified with various electron-donating (EDG) and electron-withdrawing (EWG) groups, enabling their application in a wide range of fields, including chemical sensing, biodetection, and catalysis, as illustrated in Figure 3 (Guan et al., 2023).

Figure 3. *Application fields of CQDs. Adapted from (Guan et al., 2023).*

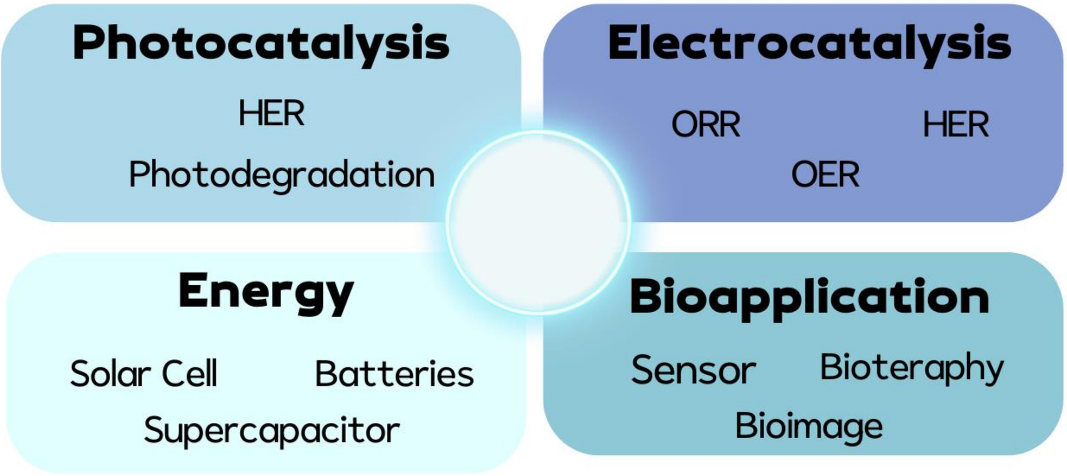

In the context of sensor technology, matrices play a critical role in determining the specificity, sensitivity, and overall performance of sensors. Matrices can be made from various materials, each of which offers unique properties tailored to different sensing applications (Ma et al., 2023). Among the most used matrices are those based on silicon, metal oxides, organics, and polymers. Among the latter group, NC stands out because of its renewable nature and unique properties, such as biocompatibility, low toxicity, and relatively low production cost. Owing to its structure, NC can be easily modified and applied as a support material in various industries (Bangar & Whiteside, 2021). Specifically, BNC, produced by bacteria of the genus *Komagataeibacter*, forms a high-purity three-dimensional network with nanoscale dimensions and excellent properties as a matrix material (Reshmy et al., 2021). Consequently, this research is promising for the development of CQD-based biosensors on polymeric cellulose matrices for mercury detection in aqueous environments. This project aims to contribute to a real-time monitoring network of HMs in aqueous effluents in the Santander region.

Research Question

What is the detection capability of Hg^{2+} in aqueous matrices for a biocomposite made of TOCN as a matrix and CQDs as a sensitizer agent?

Research Hypothesis

The fluorescence emission of a biocomposite made with TOCN and CQDs varies in response to Hg^{2+} concentration in water matrices.

1. Objectives

1.1 General Objective

- Develop a biocomposite material based on TOCN and CQDs for Hg^{2+} detection in aqueous environments.

1.2 Specific Objectives

- Synthesize and study the optical, absorption and emission properties of a biocomposite material consisting of a cellulose-based matrix with CQDs.

- Evaluate the analytical performance of the biocomposite as a sensor for Hg^{2+} detection in model aqueous samples and real contaminated matrices.

2 Reference Framework

2.1 Theoretical framework

2.1.1 Nanomaterials

Materials with sizes ranging from 1 to 100 nm (Figure 4) are referred to as nanomaterials and exhibit physical and chemical properties suitable for a wide variety of applications (Vonnie et al., 2022). Over the past decade, these nanomaterials have been implemented as analytical-grade sensors for HMs, contributing to the monitoring and protection of public health. This is because of their unique properties, such as high quantum yield (Φ), high surface-to-volume ratio, porous structures, excellent chemical reactivity, photoluminescence, and other distinctive photoelectric properties (Malik et al., 2023).

Figure 4. *Structural scales of molecules and materials. Adapted from (Padilla-vaca et al., 2018).*

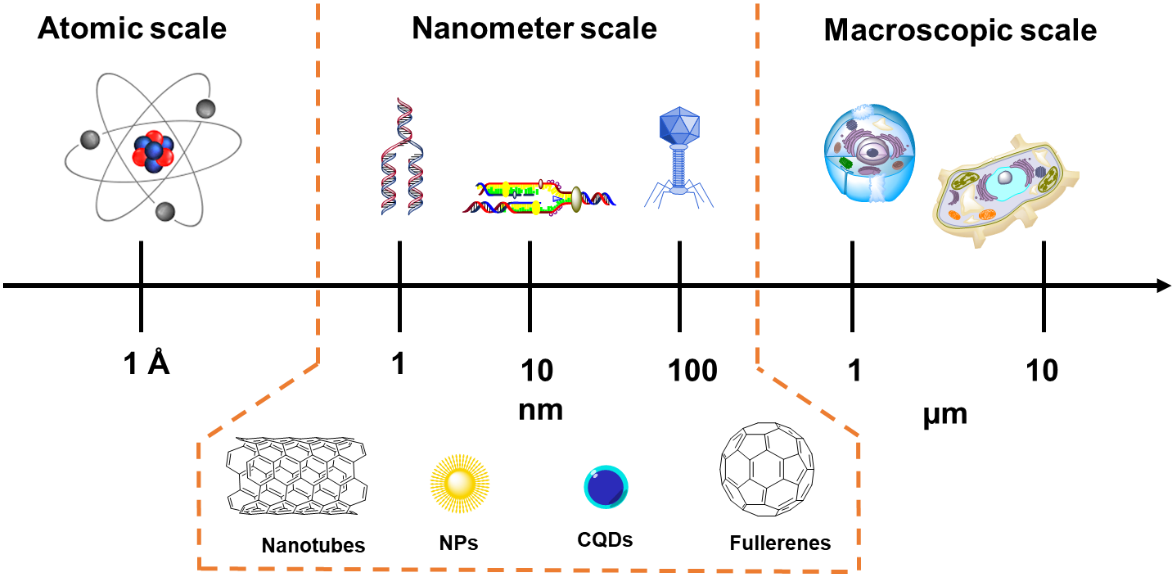

Among these properties, photoluminescence plays a central role in the selection and design of new nanomaterials with enhanced properties, as it determines the ability of a molecule to absorb photons in the ultraviolet region, excite its electrons, and ultimately emit a photon in the visible spectrum (Ding et al., 2016). If the molecule undergoes internal energy redistribution after the initial photon absorption, the emitted photon will have a longer wavelength (i.e., lower energy) than the absorbed photon (Figure 5). Special forms of photoluminescence, such as fluorescence and phosphorescence, occur when intersystem crossing leads to the transition of the electron to a state with a higher spin multiplicity (Munson et al., 2007).

Figure 5. *Diagram of the photoluminescence effect in nanomaterials, adapted from (Munson et al., 2007).*

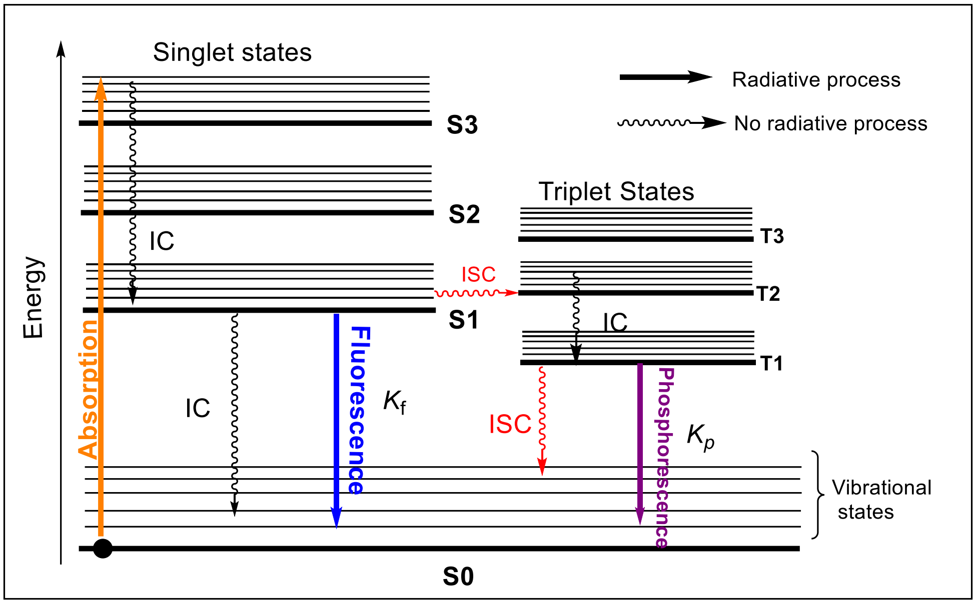

The photoluminescence effect in nanomaterials is influenced by several factors, such as the composition, structure, and size of the material, as well as the wavelength and intensity of excitation. This property is measured and utilized through optical properties, such as absorption, excitation, and emission, in the environmental monitoring of emerging pollutants (El-Shafey, 2021). This is because the excitation process is facilitated by photon absorption, which provides the energy necessary to promote electrons to higher energy states, in addition to its high sensitivity and rapid response (Zhu et al., 2023). A group of nanomaterials that has sparked significant interest in research are those derived from carbon sources, which exhibit photoluminescence, high environmental resistance, and attractive Φ, known as CQDs (Yi et al., 2022).

2.1.2 Carbon quantum dots (CQDs)

The agricultural and industrial sectors generate tons of underutilized waste annually with high carbon content because of the biotechnological processing of raw materials for product development (Sufficiency et al., 2022). This has prompted research on sustainable alternatives to mitigate the negative impacts of these waste products. Among these sustainable alternatives, a wide variety of nanomaterials have been developed that are applicable for the detection of analytes, such as HMs. Among these nanomaterials, CQDs stand out (El-Shafey, 2021), which were "accidentally" discovered by Xu et al. in 2004 while electrophoretically purifying carbon nanotubes (Xu et al., 2004).

CQDs are nearly spherical nanomaterials with a diameter of less than 10 nm, which fall under the various types of carbon dots mentioned previously (Ozyurt et al., 2023). They are synthesized either via "top-down" or "bottom-up" approaches, as shown in Figure 6. In the "top-down" method, fragmentation techniques, such as chemical oxidation, ultrasonication, and hydro/solvothermal treatment, are employed. On the other hand, the "bottom-up" approach relies on the self-assembly and polymerization of small molecular precursors using techniques like microwave processing and hydro/solvothermal treatment (Guan et al., 2023). These nanomaterials offer significant advantages, including ease of production from renewable sources, low synthesis cost, high chemical and physical stability, good electrical conductivity, low toxicity, environmental compatibility, and optical properties, like those of traditional quantum dots such as CdSe, CdTe, and gold and silver nanoparticles (Guan et al., 2023).

In In addition, CQDs can be easily functionalized with a wide variety of chemical groups, such as amines, epoxides, hydroxyls, and carboxyls, regardless of the macromolecular structure of the carbon dot (Figure 2). These surface functionalities contribute to the hydrophilic or hydrophobic nature of CQDs, as well as their behavior, size, and analytical performance, enabling them to disperse and stabilize in various solvents. Therefore, surface modification provides a way to control the properties of CQDs according to specific requirements (Mansuriya & Altintas, 2021).

Figure 6. *Synthesis categories of carbon dots, adapted from (Guan et al., 2023).*

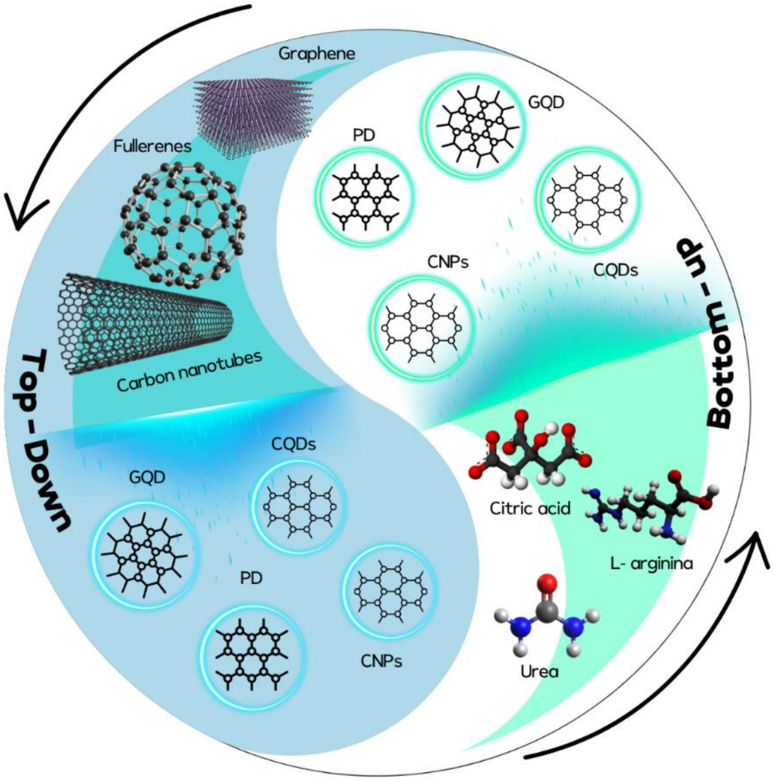

The previously discussed surface functionalities make CQDs ideal for the fabrication of detection devices (Zhu et al., 2023). Fluorescent sensors based on CQDs provide an effective and real-time method for detecting HMs that pose risks to public health and are currently detected using traditional methodologies such as AAS and ICP-MS (Kasinathan et al., 2022). It is important to highlight that for the fabrication of detection devices, it is necessary to have a matrix that enhances specificity, sensitivity, and overall sensor performance, such as a nanocellulose matrix (Ma et al., 2023).

2.1.3 Nanocellulose

NC is classified into three groups: cellulose nanofibrils (CNF), cellulose nanocrystals (NCC), cellulose nanocrystals (CNC), and BNC. Cellulose nanofibrils are obtained via enzymatic or mechanical disintegration. Cellulose nanocrystals are typically obtained by treatment with acids such as HCl or H_2SO_4. BNC is synthesized by bacterial families including *Gluconacetobacter xylinus* (Singh et al., 2021).

BNC has a high surface-to-volume ratio, high crystallinity, high strength, and low density. It is hydrophilic and can be functionalized on the surface. Because of these properties, BNC is a versatile material for incorporation into nanocomposites as reinforcement (Bangar & Whiteside, 2021). NC has a wide range of applications in the paper industry, biomedical devices, paints and coatings, electronic sensors, pharmaceuticals, construction, and packaging (Singh et al., 2021). These properties make it an excellent candidate for use as a matrix in a detection device with easy portability, as the nanocomposite formed with CQDs at the nanoscale and BCN can enhance the detection capacity of the analyte in question.

2.2 State of the art

Given the extensive versatility of NC and CQDs in their applications, scientific and industrial interest in these nanomaterials has increased over the years. By using the search query in Scopus: cellulose AND ("carbon quantum dots") AND metals, the fields with the highest number of published reports are materials science, chemistry, and chemical engineering, with China leading in publication output. However, Colombia has relatively few publications that meet the search criteria. It is important to note that there has been a rise in research in this area in recent years, as shown by the growing number of publications, although there is a noticeable bias toward publications from China. Consequently, there is a clear need to further investigate this line of research, particularly in the development of new materials for the detection of HMs.

Many applications of CQDs depend on their surface properties, yet a thorough understanding of their interactions and characteristics necessitates defining the entire structure. Consequently, some researchers have suggested utilizing graphite cores, carbon nitride, and polymeric frameworks as structural components proxies. In 2008, Bourlinos et al. described the structure of CQDs as having a carbon-rich core composed of carbonized intermediates, which is marked by a highly amorphous architecture containing both aromatic and aliphatic regions. However, structural characterization remains limited and continues to be a challenge (Mintz et al., 2019).

Concerning the chemical structure, CQDs core is commonly regarded as “carbonogenic” without further explanation, while on the surface, CQDs exhibit various functional groups such as oxygen, amino groups, or polymer chains, depending on the initial materials or dopant species. Current theories propose two types of CQD cores: crystalline graphite and amorphous cores, based on the amount of sp^2 carbon present in the core (Mintz et al., 2019).

Studies have suggested that both the conjugated π-carbon core and the functional groups on the surface contribute to photoluminescence (Mansuriya & Altintas, 2021). However, Hinterberger et al. proposed that fluorescence may originate from fluorophore molecules formed as byproducts of synthesis. However, this hypothesis does not clarify whether these fluorophores are covalently bound or adsorbed on the surface. Therefore, determining the exact composition of CQDs is hindered by the fact that reaction products often contain multiple fractions of CQDs (Hinterberger et al., 2019).

Xue et al. developed a nanopaper from carbon quantum dots and oxidized cellulose nanofibers for Fe^{3+} detection. The synthesized sensor was analyzed using TEM, SEM, XRD, FT-IR spectroscopy, XPS, CP/MAS, and NMR, and the carboxyl groups of the nanopaper were covalently bonded to the amino groups of the carbon quantum dots. In addition, the synthesized nanopaper exhibited high transparency and strong emission under ultraviolet light. The detection limit of the sensor was 10 µM, and different substrate ratios were evaluated, such as 1:1, 1:2, and 2:1, with the 1:1 ratio yielding the best results (Xue et al., 2019).

Tan et al. designed a fast and simple parallel detection method for Cd^{2+} and Hg^{2+} by using CQDs. They used L-arginine as a carbon and nitrogen source, synthesized through hydrothermal methods, and showed stable fluorescent properties that are favorable for HMs detection, with a φ of 72%. The sensor exhibited a linear detection range of 0-26.8 µM for Cd^{2+} and 0-49.9 µM for Hg^{2+}, with an emission wavelength (λ_{em}) of 354 nm and an excitation wavelength (λ_{exc}) of 295 nm. This demonstrates that CQDs can function as selective sensors for these pollutants (Tan et al., 2022).

In 2023, Jing et al. developed a bifunctional fluorescent adsorbent nanocomposite of collagen fiber/CQDs for adsorption and detection of Pb^{2+}. During the synthesis of this nanocomposite, collagen fibers were modified by carboxylation, which increased the number of active sites for Pb^{2+} ion adsorption. The construction of this nanocomposite creates a three-dimensional network, and the abundant surface groups enhance the aggregation and chelation of the metals. Therefore, the synthesis of this type of nanocomposite ensures stability and positions it as a versatile strategy for the adsorption and detection of microplastics (Jing et al., 2023).

Noun et al. conducted a series of experiments to develop concrete tools for metal detection by evaluating the quenching behavior of Hg^{2+} and Pb^{2+} cations. By analyzing each of the transitions that occur and correlating them with the functional groups of the CDs, they proposed that the availability of Hg^{2+} ions promote the formation of a CD-mercury complex. They suggested that changes in the absorbance spectra indicated that a static quenching mechanism is likely to occur in this CD system with these two metal cations (Noun et al., 2021).

Hydrothermal synthesis is one of the most used synthetic techniques. Qi et al. obtained nitrogen-doped blue-emitting CDs using citric acid and urea, with a quantum yield of 35%. CQDs can be synthesized from a wide variety of carbon sources, making these materials accessible and versatile option for numerous applications. However, this ease of production leads to an inherent challenge: understanding their behavior and properties depends on the specific structure and composition of the synthesized material. The variability in sources and synthesis methods can result in significant differences in the surface functionalization and optical and electronic characteristics of CQDs, which implies the need for in-depth and detailed studies to unravel the effect of each parameter on their behavior. Thus, although the production of CQDs is a relatively straightforward process, the complexity of their analysis and characterization remains an active area of scientific research (El-Shafey, 2021).

Experimental section

The research methodology, outlined in Figure 7 began with the synthesis of CQDs, followed by their purification using two distinct techniques: dialysis (CQDs-DL) and column chromatography (CQDs-CC). Simultaneously, the support material, BNC, was biosynthesized and subsequently oxidized to produce TOCN, serving as the matrix for the biocomposite. Both the CQDs and the TOCN were characterized regarding their structural and optical properties. The resulting biocomposite (CQDs/TOCN), a two-dimensional nanopaper, was evaluated for its Hg^{2+} detection performance in aqueous media. This evaluation was conducted using UV-Vis spectroscopy, fluorescence analysis, and ICP-OES, employing both synthetic and real environmental samples.

***Figure 7**. Methodological stages.*

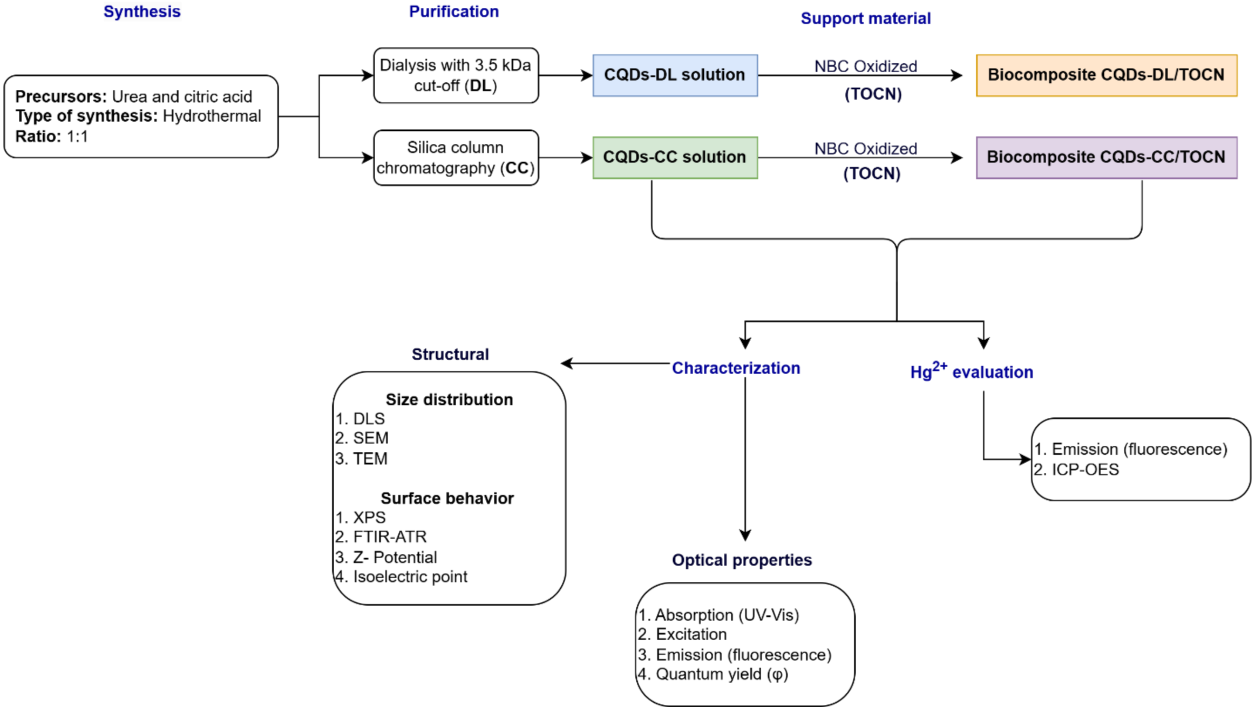

Comprehensive structural and optical characterization was performed on the CQDs, TOCN matrix, and CQD/TOCN biocomposite using various analytical techniques. Size distribution was assessed through dynamic light scattering (DLS), scanning electron microscopy (SEM), and transmission electron microscopy (TEM), yielding detailed insights into their nanostructure. Surface behavior was investigated using X-ray photoelectron spectroscopy (XPS) to identify chemical functionalities, nuclear magnetic resonance (NMR) for molecular interactions, Fourier-transform infrared (FT-IR) spectroscopy for functional group identification, zeta potential analysis for surface charge, and isoelectric point determination to evaluate surface stability. Optical properties were examined by measuring UV-Vis absorption, fluorescence excitation and emission spectra, and calculating the Φ, offering a comprehensive understanding of their optoelectronic behavior.

3.1 Materials

Citric acid (≥99%, Merck), urea (≥99%, Merck), mercuric chloride (≥99%, Merck), ethanol (≥99%, J.T. Baker), ethyl acetate (≥99%, J.T. Baker), rhodamine 6G (≥99%, Alfa Aesar), rhodamine B (≥99%, Alfa Aesar), dihydroquinine Sulfate (≥99%, USP) silica powder (60Å, Sorbtech), silica XG TLC Plates (UV254, Sorbtech®), deionized water (resist >18.2 MΩ-cm). Dialysis membrane MWCO=3.5 kDa (Thermo scientific®), membranes were used as received. Acid digestion reactor model DA 4748 (Parr®).

3.2 Synthesis of CQDs

CQDs were obtained as follows (Chaghaghazardi et al., 2023), citric acid and urea, in a 1:1 ratio (0.6 g), mixed until complete dilution in deionized water (60 mL), subsequently the dilution was transferred to the Teflon-lined autoclave and heated at 200 °C for 6h. The crude products are filtered with a 0.22 μm mixed cellulose ester filter.

3.3 Dialysis purification of CQDs: CQDs-DL

Following the purification technique most used, dialysis was carried out as follows (Chen et al., 2019). The filtered solution was purified using a 3.5 kDa dialysis membrane in double-distilled water for 72 h, making 10 water changes during the process. The resulting sample was obtained by a simple rotary evaporation operation and the brown viscous liquid product was obtained (CQDs-DL).

3.4 Column chromatography purification of CQDs: CQDs-CC

The crude reaction mixture of CQDs (Rxn) was concentrated to approximately 5 mL for fine separation. Using a mixture of ethyl acetate and ethanol as the mobile phase, the blue-emitting component was well separated. To obtain all fractions, ratios of 1:5, 0:1, and 1:1 ethanol and water were used. Purified products were obtained through a simple rotary evaporation process. The resulting dark green viscous liquid was designated as CQDs-CC. The verification of purified fractions was conducted using thin-layer chromatography (TLC) to ensure product purity and separation efficiency.

3.5. Matrix: BNC production and TOCN

BNC was obtained using Hestrin & Schramm (H-S) medium prepared in distilled water and pH adjusted to 5.0. The solution was autoclaved at 121 °C for 15 min and inoculated with 1000 µL of *Glucanoacteobacter xylinus* suspension under sterile conditions. The erlenmeyer flask was incubated at 150 rpm for 3 days at 30 °C.(Saavedra-Sanabria et al., 2021) For static fermentation, the media composed of cocoa mucilage (50%), yeast extract (12.8 g/L), ascorbic acid (7 g/L) and sodium citrate (2.7 g/L) in distilled water, adjusting the pH to 5.0. The solution was sterilized, inoculated with 10 mL of each bioreactor, and incubated for 15 days at 30 °C. Oxidized BNC (TOCN) was obtained mediated by TEMPO. BNC (1 g) was suspended in water (100 mL), TEMPO (16 mg), and NaBr (100 mg), while stirring at room temperature. NaClO (0.18 mol) was added dropwise in an ultrasonic bath (40 MHz), maintaining the pH at 10.5 with 0.5 N NaOH. After four hours, ethanol was added to neutralize the residues and terminate the reaction. Finally, the TOCN fibers were centrifuged, and a white precipitate was recovered (Gómez et al., 2017).

3.6 Biocomposite Assembly: CQDs-DL/TOCN, and CQDs-CC/TOCN

TOCN (0.4 mg dry weight) mixed with constant stirring with solutions of the CQDs: CQDs-DL and CQDs-CC. Using concentrations of 100, 50, 25, 12, 6 mg/L. The mixture was introduced into a magnetic filtration funnel (diameter 4 cm) using a mixed cellulose ester white grid filter with a pore size of 0.45 µm to perform vacuum filtration. The biocomposite films were obtained by drying at room temperature.

3.7 Structural and Optical Characterization

Fluorescence characteristics of the synthesized CQDs were detected using a 365 nm Spectroline® lamp and recorded in fluorescence spectra using a PTI/QM-40 QMatrix spectrofluorometer. UV-Vis spectra were recorded on a Thermo Scientific Genesys-50 UV-visible spectrophotometer. The functional groups of the CQDs were analyzed using a Jasco FT/IR-4X instrument. The particle size and zeta potential were measured using a Malvern ZS-90 Zetasizer ZS-90. NMR spectra were recorded using a 400 MHz Bruker Avance III spectrometer. The morphologies of the CQDs were observed by TEM using a Philips Tecnai 12 (4K FEI Eagle camara and 2K AMT camera), whereas the morphologies of the biocomposite fibers were analyzed by SEM using a JEOL JSM-7600F Tmax d'Oxford instrument. Surface composition analysis was performed by XPS using an XPS/ISS/UPS-ACentendo SPECS equipped with a PHOIBOS 150 2D-DLD energy analyzer. Finally, the concentration was quantified by ICP-OES using an Avio™ 220 Max (PerkinElmer®).

3.8 Analytical evaluation in real and synthetic samples

Solutions of CQDs-CC, CQDs-DL, and the biocomposites CQDs-DL/TOCN, CQDs-CC/TOCN were immersed directly in the mercury solution to simulate the *in-situ* operation. Consequently a 96-well microplate was used to put biocomposites in contact with $HgCL_2$ solution at concentrations ranging from 1 mM to 1 nM ($272 – 2.7x10^{-4}$ mg/L). Real samples were taken from the Surata River (coordinates: 7.1816978, - 73.0784003 Vereda Capillabaja-Vía Surata. Colombia. The real sample was exposed to both solutions and the biocomposites of CQDs, each prepared at a concentration of 100 mg/L. The response of the solutions and biocomposites was evaluated using fluorescence spectra and compared with the detection limit of conventional methods, such as ICP-OES.

Results and Discussion

Structural Comparison of Synthesized CQDs-DL and CC

The structural comparison of the synthesized DL- and CC-CQDs through dynamic light scattering (DLS) analysis and transmission electron microscopy (TEM) revealed distinct differences in the particle size distributions (see Figure 8). Both types of CQDs showed similar size distributions at concentrations above 12 mg/L; however, a significant difference was noted at a concentration of 6 mg/L. At this lower concentration, the dialyzed CQDs displayed a particle size distribution centered around 1.0 nm, while the column-purified CQDs-CC showed a particle size distribution centered around 1.7 nm.

The size distribution histograms generated from the TEM images were consistent with the DLS results, demonstrating similar trends (see Figure 8b and 8d). Furthermore, direct visualization of the TEM images at a 400 nm scale revealed agglomeration in the CQDs-CC, while the CQDs-DL displayed a clearer and more uniform distribution. These observed agglomerations adjust with the particle size distributions. The size distribution observed for CQDs-CC shows an average of 4.7 nm, whereas CQDs-DL exhibit an average size of 5.4 nm.

In the DLS plots, volume measurements show an increase for particles smaller than 2 nm. This increase can be understood by reviewing the principles of Rayleigh and Mie scattering theories, which explain how light interacts with particles of different sizes (Akimov, 2024). According to the Rayleigh theory, the intensity of scattered light is sensitive to small variations in particle size, especially for particles much smaller than the wavelength of the incident light. For particles under 2 nm, the assumptions of these theories may not hold, leading to discrepancies in the volume estimates derived from DLS data. Mie theory, which applies to larger particles, indicates that as particles approach or exceed the wavelength of light, their scattering characteristics change significantly, further complicating the interpretation of DLS measurements (Craig F. Bohren, 1998).

Figure 8. *Size distribution of both CQDs. a) Size distribution of CQDs-DL obtained from DLS measurements; b) TEM images of CQDs-DL, along with a size distribution histogram calculated from TEM results; c) Size distribution of CQDs-CC obtained from DLS measurements; d) TEM images of CQDs-CC, accompanied by a size distribution histogram calculated from TEM results.*

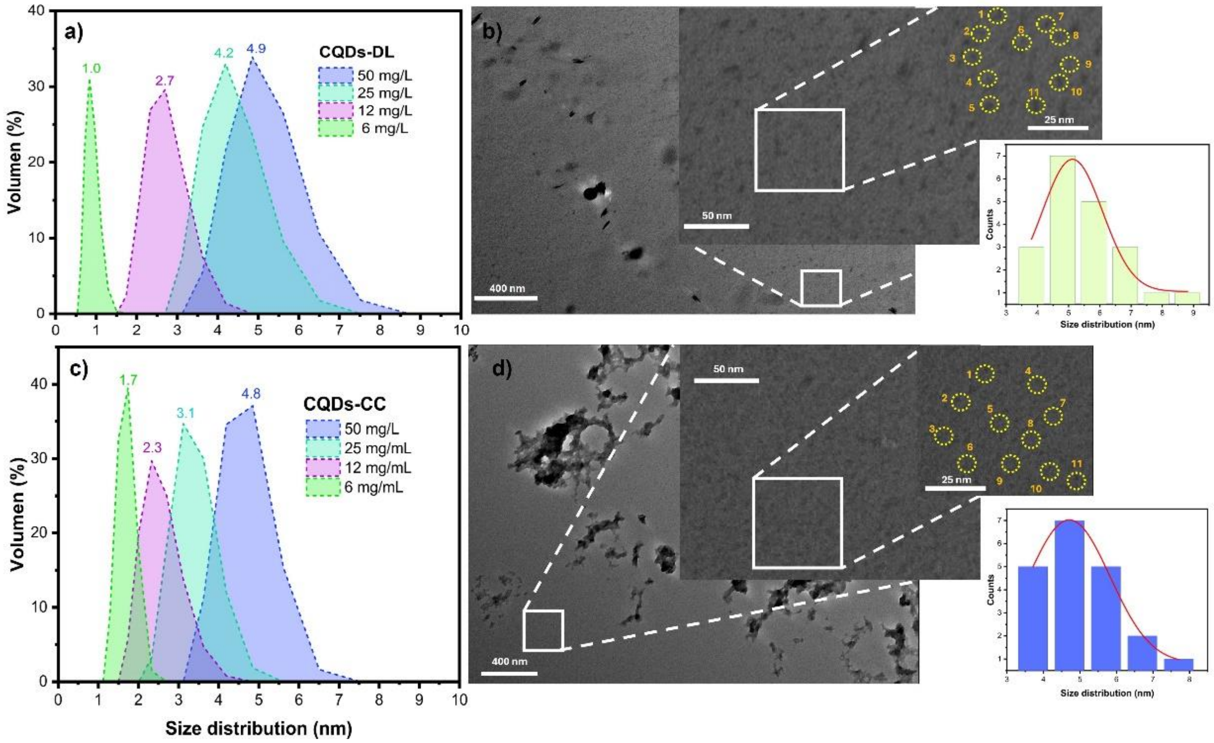

The general XPS spectra analysis indicates that both CQDs share a similar composition of carbon and oxygen, suggesting comparable surface functionalities. However, the difference in the binding energies (BE) of the nitrogen signals implies variations in the chemical environment of nitrogen between the two samples. This shift may be attributed to the different bonding states or nitrogen-containing functional groups, which could influence the electronic properties and overall reactivity of CQDs (Giordano et al., 2023; Yadav et al., 2023).

Elemental composition analysis showed that the carbon content was higher in CQDs-CC (70%) than in CQDs-DL (66%), oxygen content between the two samples was 25% for the CQDs-CC and 27% for the CQDs-DL. Difference was observed in the nitrogen content, which was slightly higher in the CQDs-DL (5.76%) than in the CQDs-CC (4.95%). To explain the variations in elemental composition and functional groups, it is important to consider the purification method

(Chen et al., 2019). The dialysis method separated the CQDs based on size, allowing larger particles enriched with nitrogen-containing functional groups, such as amines (NH_2) and protonated amines (NH_3), to remain in the solution. The retention of larger CQDs during this process likely contributed to the higher nitrogen content observed in the CQDs-DL (Kong et al., 2024). The presence of these functional groups on the surface could hinder the filtration of larger particles through the dialysis membrane (3.5 kDa), resulting in a sample that is not only enriched in nitrogen but also in surface functionalities that may enhance reactivity and solubility (Chang et al., 2022).

In contrast, CQDs-CC utilizes ethanol in the mobile phase, which influences separation based on both size and charge interactions with the stationary phase. The polar nature of silica have strongly retained CQDs with higher surface charge owing to their functional groups, resulting in the preferential elution of smaller particles with fewer nitrogen functionalities (G. Sharma et al., 2017). Consequently, the lower nitrogen content in CQDs-CC can be attributed to the retention of larger CQDs in the column, which have had significant interactions with silica because of their higher charge density.

Figure 9. *Surface behavior of both CQDs. High- resolution XPS of a) C1s spectra of CQDs-CC; b) N1s spectra of CQDs-CC; c) O1s spectra of CQDs-CC; d) C1s spectra of CQDs-DL; e) N1s spectra of CQDs-DL; f) S O1s spectra of CQDs-DL; g) zeta potential of both CQDs; h) isoelectric point of both CQDs; i) FTIR spectra of both CQDs.*

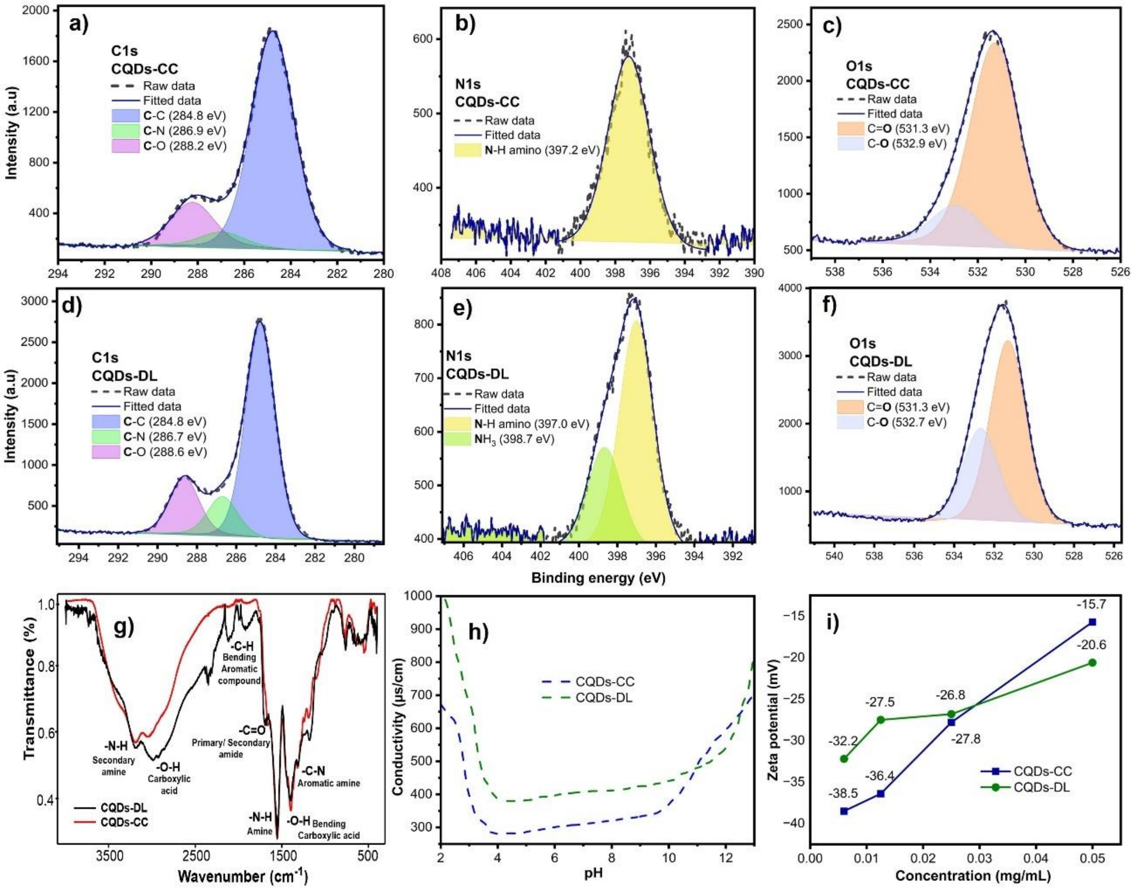

The presence of $-NH_2$ and-NH_3 groups in the CQDs can be inferred from the high nitrogen content and specific BE values observed in the XPS analysis (Figure 9b and e). Nitrogen atoms in amines typically exhibit BE around 399.5 eV(Lazar et al., 2019), while those in protonated amines are often found at slightly higher binding (Bao et al., 2023). This suggests that the nitrogen signals in CQDs-DL (Figure 9e) at 397.0 eV and 398.7 eV correspond to amine and protonated amine functional groups, respectively. Additionally, the observed carbon-to-nitrogen ratio and BE values indicated the presence of imine group in the structural backbone of the CQDs (Lazar et al., 2019). Imine group typically exhibits a BE in a similar range 397.9 eV, further supporting the notion that nitrogen is incorporated into the CQDs architecture in various forms.

The differences in the purification methods reveal critical insights into CQDs properties. While dialysis appears to favor larger nitrogen-rich CQDs, CQDs-CC selectively elude smaller particles, resulting in a fraction with a reduced percentage of nitrogen. Functional groups, such as NH_2, NH_3, and potentially imines, underscore the complex chemistry of CQDs and their implications for electronic properties and reactivity. These observations highlight the importance of purification techniques in influencing the final composition and properties of CQDs, ultimately affecting their potential application in various fields (Wang & Hu, 2014). Infrared spectra (IR) (Figure 9g) confirmed the XPS analysis and supported our hypothesis regarding the structural surface composition and arrangement. N-H signals at 1680 cm^{-1} (primary amine) and 3190 cm^{-1} (secondary amine), as well as the C-N signal at 1190 cm^{-1} (aromatic amine), are consistent with the XPS BE results. Meanwhile, the oxygen composition was evidenced by the O-H bending signal at 1400 cm^{-1} and the O-H stretching signal at 3000 cm^{-1}, corresponding to carboxylic acid. A notable signal at 1685 cm $^{-1}$ corresponds to primary and secondary amides, explaining the XPS BE energy at 531.3 eV (Figure 9f) for the C=O group (carbonyl). The IR spectra also revealed bending signals corresponding to aromatic compounds, which represented the CQD backbone structure.

The conductivity and Z-potential plots (Figure 9h and 9i), suggest that the CQDs-CC are more stable and less reactive than CQDs-DL. The Z-potential of CQDs-CC at lower concentrations (30 mg/L shows a noticeable increase in magnitude, while the Z-potential of CQDs-DL at the same concentration also showed an increase, although less pronounced compared to CQDs-CC. This difference may be due to an excess of positive surface charges from NH_3 groups, further confirming the XPS analysis. Moreover, at an acidic pH, the conductivity measurements indicated that the CQDs-DL exhibited greater conductivity than the CQDs-CC. This increased conductivity attributed to the higher concentration of positive surface charges on the CQDs-DL, resulting from the protonation of the amine groups ($-NH_2$ to $-NH_3^+$) under acidic conditions.(Chaghaghazardi et al., 2023) Additionally, the presence of carboxylic acid groups (–COOH) in the CQDs-DL also contribute to the conductivity, as these groups can remain protonated in acidic environments, further enhancing the overall ionic strength of the solution. The combination of these positively charged species promotes the mobility of ions, leading to higher conductivity in the CQDs-DL than in the CQDs-CC.

Furthermore, the isoelectric point (Figure 9h) indicated that the curves stabilized from pH 4 to 10 for CQDs-CC and from pH 4 to 12 for CQDs-DL, demonstrating a range in which the particles maintain relatively stable conductivity. This stabilization advises that both types of CQDs may exhibit buffering effects because they can resist changes in pH within these ranges. Notably, the CQDs-DL displayed a broader range of stable conductivities, which can be attributed to the higher number of ionizable groups present on their surface compared to the CQDs-CC. The increased presence of ionizable groups enhances the buffering capacity of the CQDs-DL, allowing them to better maintain a consistent ionic environment, especially near the isoelectric point, which is approximately pH 6.5 CQDs-CC and 7.5 CQDs-DL, further emphasize the role of purification in defining the electrochemical behavior and properties, highlighting the differences in surface chemistry and stability between the two types of CQDs.

Optical properties

Surface topology plays a crucial role in the optoelectronic behavior of both types of CQDs, particularly influencing their excitation and Φ. Comparing spectra with the literature, the absorption, emission, and excitation bands agreed (Wang & Hu, 2014). Typically, the size of the CQDs, the presence of emissive traps, and quenching states mainly affect the excitation and emission bands (Yadav et al., 2023). By analyzing the HOMO-LUMO band gap and its relationship with excitation and particle size, for graphene fragments, we can infer that, given the similar chemical structures and behaviors of CQDs, there is congruence between size and excitation energy (Li et al., 2010). Therefore, CQDs-DL are easier to excite than CQDs-CC.

The absorbance and emission spectra (Figure 10) revealed that both samples emitted light at similar wavelengths, albeit with different intensities. For CQDs-DL, excitation occurred at a shorter wavelength (321 nm, see Figure 10c), whereas for CC-CQDs, excitation occurred at a longer wavelength (362 nm, see Figure 10b). This shift indicates differences in the electronic environment, driven by the distinct surface functional groups.

Figure 10. *Absorption, excitation, and emission spectra of a) Rxn of CQDs, b) CQDs-CC, and c) CQDs-DL.*

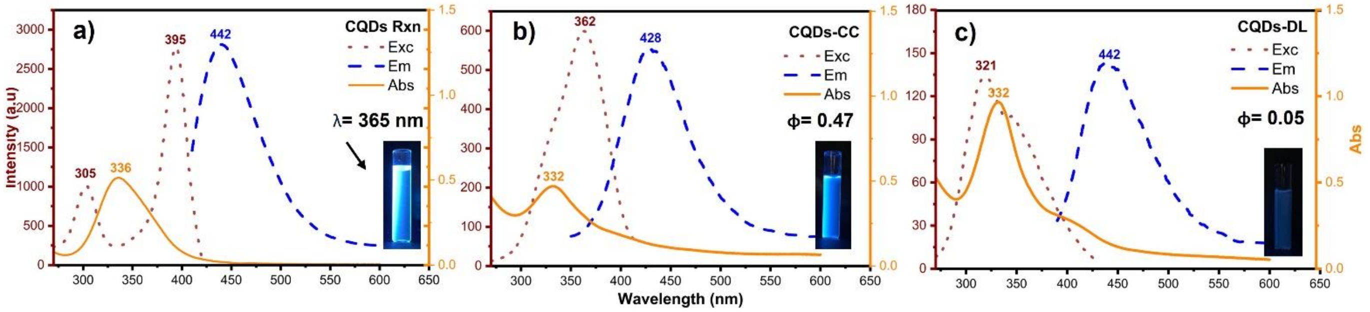

CQDs-DL, which contained a higher concentration of NH_2 and NH_3 groups along with imine-like structures, as confirmed by XPS analysis, exhibited both bathochromic and hypsochromic shifts. Surface defects or functional groups in the CQDs-DL lead to electronic states that absorb more energy but release less radiatively, as reflected by their lower Φ (0.05).

In contrast, the CQDs-CC, with a lower amount of NH_3 and imine-related groups, and predominantly NH_2 groups on its surface, achieved a much higher Φ (0.47). This minimizes nonradiative decay processes, enhancing the efficiency with which the absorbed energy is converted into emitted light. Although both CQDs emit at similar wavelengths (428 nm for CQDs-CC and 442 nm for CQDs-DL), the difference in quantum yield highlights the significant impact of surface chemistry on emission efficiency.

This richer chemical composition results in greater surface conductivity in CQDs-DL due to increased polar interactions and the presence of electron-donating groups, such as NH_3. However, this enhanced conductivity comes at the cost of quantum efficiency, as these functional groups promote nonradiative relaxation pathways (Anpalagan et al., 2024). The difference in Φ between the two samples can be attributed to the prominence of surface defects in the CQDs-DL. These defects act as traps for excitons, facilitating non-radiative decay through vibrational modes or other non-emissive processes (Zheng et al., 2020). In contrast, the cleaner surface of the CQDs-CC enables more efficient radiative recombination, which is why it displays higher Φ.

Structural comparison of biocomposite

The structural characteristics of the biocomposite obtained for the development of detection devices. A matrix was specifically designed to enhance sensor specificity, sensitivity, and overall performance (Lv et al., 2022). This support material was derived from TOCN, and the XPS C1s spectrum reveals characteristic interactions, including C-C (284.8 eV) and C-OH (286.8 eV). Furthermore, BNC was oxidized via TEMPO to improve functionalization at the C_6 position of BNC (Martínez-Ramírez et al., 2023). The high-resolution C1s XPS spectrum (Figure 11b), displays the oxidation markers: C-C (284.8 eV), C-O (286.5 eV), and O-C=O (288.1 eV), the latter confirming the successful oxidation process (Martínez-Ramírez et al., 2023).

Subsequent analysis of the biocomposites is shown in Figure 11c. The C1s spectrum indicates the presence of C-C (284.8 eV), C-N (287.3 eV), C-O (287.8 eV), and O–C=O (289.4 eV). Figure 11c shows the presence of C-N bonds, indicating the interaction between nitrogen from the CQDs and the biocomposite surface. This observation confirms that nitrogen from the CQDs is integrated into the structure of the biocomposite, suggesting its incorporation primarily on the surface (Martínez-Ramírez et al., 2023; Subbotina et al., 2022).

The emission spectra (Figure 11d) reveal two distinct maxima at 420 and 442 nm for the biocomposite. The emission peak at 442 nm, characteristic of Rxn in solution, suggests that the emission at 420 nm is due to electronic interactions between the CQDs and TOCN, which modify the electronic environment (Calderón-Vergara et al., 2020). Given the particle sizes of the CQDs and the fiber dimensions of the TOCN, it is plausible that the CQDs are incorporated both within the TOCN, forming an internal matrix, and on their surface, where they contribute to surface functionalization. This structure significantly increased the reaction surface area (Subbotina et al., 2022). Additionally, the emission spectrum of NC, observed at 570 nm, did not interfere with the biocomposite performance. Overall, these findings demonstrate that the structural and optical properties of the biocomposite are strongly influenced by the functionalization BNC and the incorporation of CQDs. The nanofibrillar structure coupled with well-defined emission characteristics suggests that this material is well suited for enhanced detection device performance (Lv et al., 2022).

The SEM images in Figure 11e illustrate TOCN fibers morphology, revealing individual fibrils with nanometric dimensions (32, 28, 20 nm). The nanoscale structure contributes to the enhanced surface area and performance of the biocomposite in sensor applications (Isogai et al., 2011).

Figure 11. *Structural behavior of biocomposites. a) high-resolution XPS C1s spectra of NBC, b) high-resolution XPS C1s spectra of TOCN, c) high-resolution XPS C1s spectra of biocomposite, d) emission spectra of TOCN and CQDs Rxn/TOCN and the cellulose was excited at 530 nm, different from the CQDs, e) SEM image of biocomposite, f) Physical appearance of the TOCN under UV (365 nm) and g) Physical appearance of the biocomposite of CQDs Rxn/TOCN under UV (365 nm).*

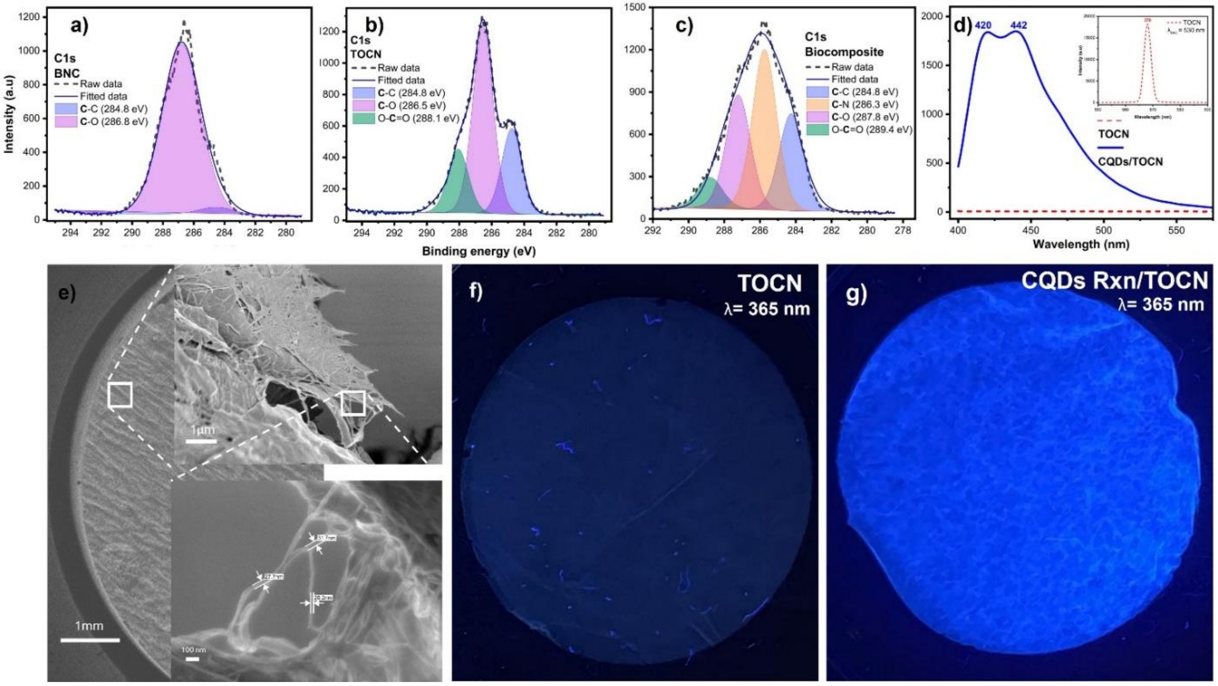

Analytical response of CQDs and biocomposites: synthetic and real sample

The Rxn was evaluated against seven solutions containing HMs to evaluate its response as shown in Figure 12a. Subsequently, purified CQDs (CQDs-CC and CQDs-DL) and their respective biocomposites were evaluated in synthetic $HgCl_2$ solutions at various concentrations. These materials were applied to a real sample to assess their performance under practical conditions. A significant decrease in fluorescence was observed when the Rxn was in contact with Hg^{2+} 1 mM (272 mg/L) indicating a selective quenching effect.(Noun et al., 2021) This selective behavior prompted further analysis by calculating the relative fluorescence intensity (I/Io) of the CQDs-CC (Figure 12b) and CQDs-DL (Figure 12c). For both types of CQDs, the most pronounced fluorescence quenching was observed with Hg^{2+}, although other metals, such as Pb^{2+}, Co^{2+}, Ni^{2+}, Ag^{+}, Cd^{2+}, and Cu^{2+}, induced varying levels of fluorescence quenching. When comparing the two CQDs, it was evident that CQDs-DL exhibited a stronger quenching response to mercury than CQDs-CC, suggesting that DL-CQDs are more selective for Hg^{2+}. However, for the other metals, both CQDs displayed relatively similar selectivity based on the changes in fluorescence intensities. Interestingly, CQDs-CC showed selectivity for Cu^{2+} after Hg^{2+} exposure, whereas CQDs-DL were more selective for Pb^{2+} following mercury exposure. The consistent detection pattern and intensity reduction observed across different HMs suggest that the purification method can be strategically optimized to fine-tune the detection selectivity of the CQDs rationally.

The enhanced quenching effect in CQDs-DL suggests that these functional groups provide more binding sites and better coordination with mercury, facilitating a more efficient energy-transfer process that leads to fluorescence quenching (Noun et al., 2021). In contrast, CQDs-CC contain a higher presence of NH_2 groups but lack the same level of complexity in their surface chemistry, limiting their quenching efficiency (Elmizadeh et al., 2019). The key insight here is that the functional groups present on the surface of CQDs significantly influence their metal-ion sensing performance (Mudasir et al., 2020). The presence of nitrogen groups in CQDs-DL enhanced the interaction with Hg^{2+} ions, resulting in more pronounced fluorescence quenching than in CQDs-CC.

At first observation, it could be inferred that CQDs-DL present a more favorable option. However, when comparing all the optoelectronic properties, including fluorescence performance, emission, and the energy required for excitation, and considering that the CC purification technique offers greater control over the selection of the quantum dot fraction, it becomes clear that CC-CQDs represent a highly effective choice.

Figure 12. *Fluorescence response and relative fluorescence intensity for HMs. a) Physical appearance of the CQDs solution (0.1 mg/mL) vs. HMs under UV (365 nm) and natural light, relative fluorescence intensity (I/Io), b) CQDs-DL, and c) CQDs-CC.*

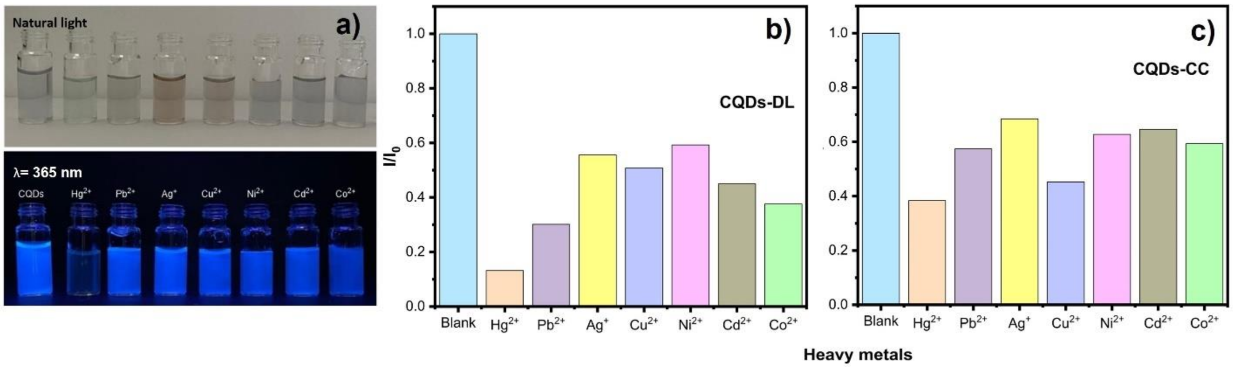

Finally, the LOD was determined for each case, given the sensitivity of both the CQDs to Hg^{2+}. Figure 13a shows the analysis conducted in different wells with CQDs-CC solutions ranging from 100 mg/L to 6 mg/L. Hg^{2+} solutions were subsequently added to these wells (Figure 13b) and the samples were observed under UV light (365 nm). A significant decrease in fluorescence was observed, particularly for the two highest mercury concentrations, indicating that CQDs-CC effectively quenched fluorescence in response to Hg^{2+} concentration. This observation was corroborated by the emission spectra in Figure 13c, where the quenching curve for CQDs-CC is plotted against varying Hg^{2+} concentrations. As shown, the greatest quenching occurred at the highest concentration of 272 mg/L, followed by 27.2 mg/L, 2.7 $x10^{-2}$mg/L, and a consistent quenching effect for concentrations as low as 0.027 mg/L and $2.7x10^{-4}$ mg/L.

The behavior of the CQD-CC/TOCN biocomposite was also evaluated in Figure 13d), and it demonstrated a similar response pattern. However, it is worth noting that the fluorescence intensity was not identical to that of the CQDs-CC in solution, showing a more discrete response for the first two Hg^{2+} concentrations, followed by a consistent behavior for the remaining concentrations. This suggests that the presence of the NC matrix in the biocomposite alters the quenching dynamics, owing to the interactions between the TOCN and CQDs-CC.(Zou et al., 2020) The strong fluorescence response of CQDs-DL is demonstrated in Figure 13e and 13f, showing a noticeable difference in fluorescence under UV light compared to that of CQDs-CC. However, Figure 13g reveals that CQDs-DL do not exhibit the same linearity in fluorescence quenching across varying Hg^{2+} concentrations as observed in CQDs-CC. This nonlinear behavior can be attributed to the more complex and charged surface chemistry of the CQDs-DL. These functional groups likely induce more variable interactions with Hg^{2+} ions, resulting in less consistent fluorescence quenching (Noun et al., 2021). A similar nonlinearity was observed in the biocomposite containing CQDs-DL (Figure 13h), where two emission peaks at 420 nm and 442 nm were recorded. This dual-emission pattern corresponds to the results in Figure 11e, where the biocomposite shows comparable peaks, potentially due to electronic interactions between the CQDs and the cellulose matrix.

The analysis highlights the distinct behaviors of CQDs-CC and CQDs-DL, which are influenced by their purification methods. CQDs-CC exhibited a more predictable and consistent quenching response across various mercury concentrations, making them potentially more dependable and accurate for quantitative detection. In contrast, CQDs-DL, purified through dialysis, demonstrated stronger fluorescence quenching (Figure 12b), although with nonlinear quenching behavior, likely due to its more complex surface chemistry. These differences emphasize the critical role of surface functionalization and purification techniques in the design and application of CQDs for heavy metal detection (Escandar & Olivieri, 2022). The limits of detection (LOD) for CQDs-CC and CQDs-DL were 1 µg/L (0.001 mg/L) and 2 µg/L (0.002 mg/L), respectively.

Figure 13. *Fluorescence response for CQDs-CC, CQDs-DL and biocomposites. a) Wells before* Hg^{2+} *contact under UV light (365 nm) of CQDs-CC, b) Wells after* Hg^{2+} *contact of CQDs-CC, c) Fluorescence response of CQDs-CC to* Hg^{2+} *solutions, d) Fluorescent response of CQDs-CC/TOCN to* Hg^{2+} *solutions, e) Wells before* Hg^{2+} *contact with CQDs-DL; b) Wells after* Hg^{2+} *contact with CQDs-DL; c) Fluorescent response of CQDs-DL to* Hg^{2+} *solutions, d) Fluorescent response of CQDs-DL/TOCN to* Hg^{2+} *solutions.*

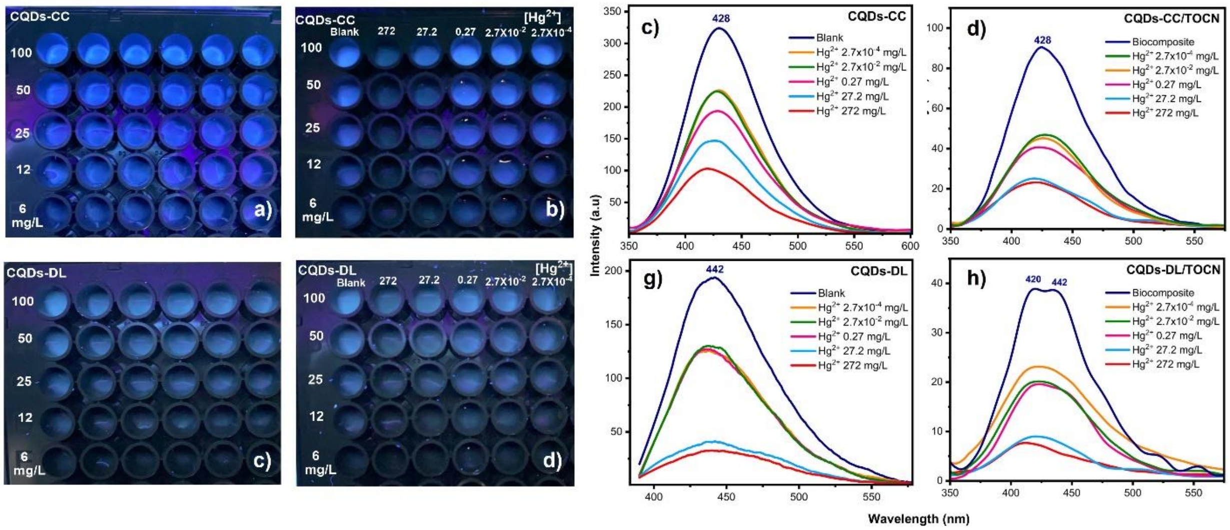

To evaluate the sensor performance, both CQDs (CQDs-CC and CQDs-DL) and their biocomposite, using an environmental sample. This study focuses on addressing Hg^{2+} contamination in water sources, particularly in regions affected by artisanal mining practices. Water samples were collected from the Surata River, specifically from the Capilla Baja sector (Colombia, coordinates: 7.1816978, –73.0784003), as shown in Figure 14a. ICP-OES analysis determined that the total mercury concentration in this water source was 0.812 µg/L.

Fluorescence response of the CQDs solution vs. real sample is shown in Figure 14b. For CQDs-CC, a noticeable decrease in fluorescence intensity was observed, accompanied by a bathochromic shift in the emission maximum from 428 to 446 nm. This shift indicates the presence of Hg^{2+} and highlights the influence of additional components in the real sample that may interact with the CQDs, potentially altering their photophysical behavior. These interactions should be considered in complex matrices (A. Sharma et al., 2019). Similarly, the CQDs-DL also exhibited a reduction in fluorescence intensity, although to a lesser degree than the CQDs-CC, and a smaller shift from 442 to 446 nm was observed.

Interestingly, both CQDs converged at the same emission wavelength with similar intensity, despite the initial differences in their fluorescence behavior in the synthetic samples. Although the differences in spectral shifts and relative fluorescence intensities vary between the two types of CQDs, the final detection response with the real sample was similar for both. This convergence could indicate that, despite variations in surface chemistries and quenching efficiencies, both CQDs achieve comparable detection outcomes in complex matrices.

A fluorescence quenching response in similar regions and toward Hg^{2+} was anticipated, given that both CQDs share the same chemical nature. As shown in the absorbance, excitation, and emission results, the emissions remained within the same wavelength range, with only subtle changes in the intensity and excitation wavelengths. From an energy perspective, these findings can guide the rational design process for developing CQDs with improved LOD and scalable industrial potential for diverse applications and environments. Moreover, these results confirm that both CQDs are stable and suitable for detecting Hg^{2+} in real samples, even within the complexity of environmental matrices.

When comparing these results to those from synthetic mercury solutions, such as those in Figure 13c and 13g, a disparity in fluorescence intensities was evident. Although the emission maxima did not shift, their intensities were lower. Specifically, the difference between the real and synthetic samples was quantified to be 72 a.u. for CQDs-CC and 10 a.u. for CQDs-DL. This difference can be attributed to the unique nature of CQDs, which are known to be stable in solution, but experimental observations show that once dried, their fluorescence diminishes upon re-dissolution, likely due to agglomeration. This aggregation disrupts their fluorescence properties, whereas in solution, these CQDs remain stable, maintaining their emission characteristics (R. Guo et al., 2019). Highlighting this stability underlines the importance of preserving the CQDs in solution for reliable sensor performance.

***Figure 14**. Real sample response. a) Geolocation of the real sample taken from the Surata River, Fluorescent response versus a real sample of b) CQDs solutions, and c) Biocomposites.*

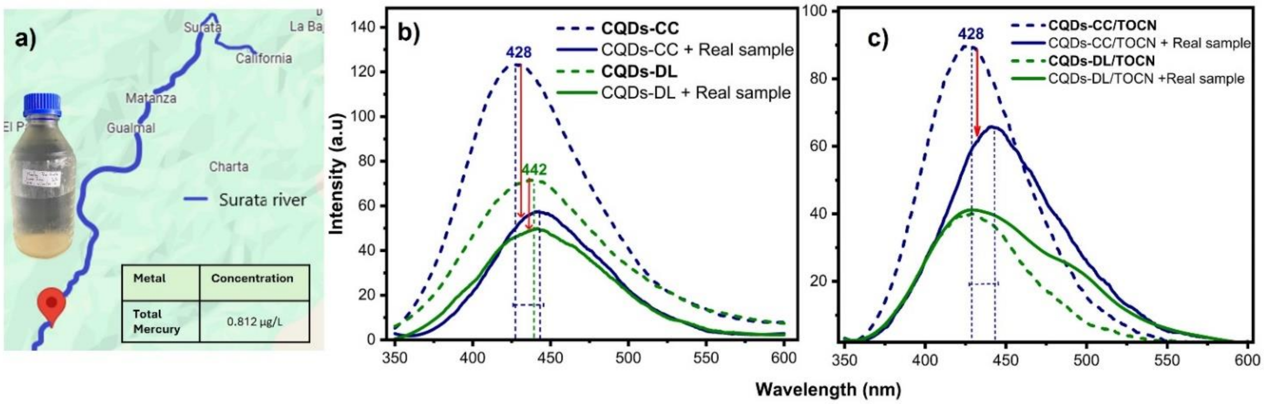

In Figure 14c, a further bathochromic shift for CQDs-CC from 428 to 443 nm was noted, while the CQDs-DL remained at its initial position. This differential response suggests that while the biocomposites (CQDs-CC/TOCN and CQDs-DL/TOCN) offer potential for detection, they do not outperform CQDs in solution when applied to real-world samples. The solution-based CQDs exhibited more pronounced shifts and intensity changes, suggesting a more straightforward interaction mechanism. As a new material, the biocomposite introduces multiple interaction possibilities between the TOCN and CQDs.

Overall, the results demonstrate that while both CQDs-CC and CQDs-DL are effective for mercury detection, especially in synthetic samples, their behavior in real environmental samples shows differences in sensitivity and response mechanisms. CQDs-CC stands out for its more prominent bathochromic shift and quenching response, suggesting its greater utility in practical sensing applications. However, the stability of these quantum dots in solution is a critical factor in ensuring reliable long-term performance, as the drying and re-dissolution processes can significantly impact their fluorescence properties.

Conclusions

The profound impact of the purification methods on the optical properties, surface chemistry, and sensing capabilities of CQDs. When CQDs purified via dialysis (CQDs-DL) displayed a more complex and charged surface composition, characterized by higher concentrations of NH_2, NH_3, and imine groups, which contributed to stronger fluorescence quenching. In contrast, CQDs purified by column chromatography (CQDs-CC) contained NH_2 groups and exhibited more predictable, linear fluorescence quenching, particularly in response to Hg^{2+}.

These distinctions in surface chemistry and structure, which are closely to their purification process, had a significant impact on the optical behavior and sensor performance of the CQDs. Dialysis, although a commonly used method for CQDs purification, has been proven to offer a coarser separation process, leading to CQDs with variable surface chemistry and nonlinear sensing responses. In contrast, column chromatography enables more precise control over surface functionalization, resulting in CQDs with consistent and reproducible optical properties. This makes CQDs-CC particularly suitable for sensitive and accurate applications in heavy metal detection, such as Hg^{2+} sensing, in which consistent responses are critical for quantitative analysis.

Furthermore, the integration of CQDs into TOCN-based biocomposites introduces additional complexity to the fluorescence response, highlighting the influence of interactions between the CQDs and the support matrix. This suggests that CQDs in solution may offer more reliable performance for real-time detection applications.

While CQDs-DL exhibited stronger fluorescence quenching, CQDs-CC demonstrated greater consistency and linearity, making them promising candidates for mercury detection and other sensor applications. Future work should focus on further optimizing the purification techniques, exploring real-world applications, and developing portable devices for on-site environmental monitoring.

Recommendations

Future research could explore promising directions. First, advancing hybrid purification techniques may yield CQDs with more precisely tailored surface functionalities, further improving their sensitivity and selectivity for detecting a broader spectrum of heavy metal ions. Extending this work to real-world environmental samples, such as water from mining-impacted regions, would offer valuable insights into the practical applicability and robustness of CQDs for in-field detection. Investigating the long-term stability and reusability of CQDs, both in solution and within biocomposite matrices, is crucial for developing sustainable and cost-effective sensor platforms. Additionally, integrating CQDs into portable sensing devices, such as microfluidic systems or sensor arrays, could enable real-time on-site monitoring of heavy metal contamination in water sources. By refining CQD design, detection strategies, and device integration, these materials hold significant potential to address pressing environmental issues, such as mercury pollution from artisanal mining, and to provide impactful, practical solutions for affected communities.

Scientific production

1. **Oral presentation**
    1.1. **Title:** Real-time Mercury Detection in Aqueous Environments using an Oxidized Bacterial Nanocellulose and Carbon Quantum Dots Biocomposite
    1.2. **Authors:** Laura Rojas-Palomino, Carlos Martínez-Bonilla, Cristian Blanco-Tirado, Marianny Y. Combariza
    1.3. **Date:** 18-23 Agosto de 2024.
    1.4. **Event:** 32nd International Materials Research Congress.
    1.5. **Place:** Sociedad Mexicana de Materiales, Cancún, México.
2. **Poster presentation**
    2.1. **Title:** Puntos Cuánticos de Carbono ¿un enrejado poliaromático?: Realidades sobre su Estructura y Métodos de Purificación
    2.2. **Authors:** Laura Rojas-Palomino, Mauricio Cerón, Carlos Martínez-Bonilla, Marianny Y. Combariza

2.3. **Date:** 02-06 Octubre de 2023.

2.4. **Event:** XIX Congreso Colombiano de Química.

2.5. **Place:** Universidad de los Andes, Bogotá, D.C.

3. Scientific article

3.1. **Title:** Insights into the Role of Purification Technique Selection for Carbon Quantum Dots: Environmental Detection of Mercury Pollution

3.2. **Authors:** Laura Rojas-Palomino, Carlos Martínez-Bonilla, Cristian Blanco-Tirado, and Marianny Y. Combariza,

3.3. **Journal:** Journal of Materials Chemistry C, Royal Society of Chemistry (RSC).

3.4. **State:** draft

Appendix

Appendix 1. XPS general composition data.

The XPS analysis provides a detailed characterization of the sample's surface composition. This section presents the general elemental composition, peak positions, full width at half maximum (FWHM), and atomic percentages obtained from the deconvoluted spectra. Additionally, the raw data is included to ensure transparency and reproducibility of the results.

Table S 1. *XPS general composition data Obtained from different samples.*

Sample	**Name**	**Position**	**FWHM**	**Raw Area**	**%At Conc**
CQDs-DL	C 1s	284.8	3.0	67433.9	66.8
	O 1s	531.8	3.4	66911.6	27.4
	N 1s	400.8	3.1	9608.1	5.8
CQDs-CC	C 1s	284.8	3.1	60421.5	70.1
	O 1s	531.8	3.5	51858.9	24.9
	N 1s	399.8	3.0	7041.8	5.0
BNC	C 1s	284.8	3.6	139501.2	62.9
	O 1s	531.8	2.8	85079.5	37.1
	N 1s	-	-	-	-
TOCN	C 1s	284.8	3.4	85780.7	38.6
	O 1s	531.8	2.5	141040.3	61.4
	N 1s	-	-	-	-
Biocomposite	C 1s	284.8	4.2	117102.2	53.6
	O 1s	531.8	2.8	102555.7	45.3
	N 1s	381.8	2.6	1071.8	1.2

Appendix 2. Dialysis performance.

Figure S 1 illustrates the physical and spectral changes observed during the dialysis process. Figure S 1(a), (b), and (c) depict the initial physical appearance of the system at time 0, immediately upon contact with water. Figure S 1(d) and (e) show the physical state of the dialysis setup after 72 hours, highlighting the observable changes in fluorescence intensity over time. Figure S 1(f) presents the emission spectra of both the dialysate water changes and the dialyzed product (CQDs-DL), demonstrating that the most fluorescent families of CQDs migrate first, resulting in the dialyzed product exhibiting significantly reduced fluorescence emission. Finally, Figure S 1(g) displays the physical appearance of the water changes and the CQDs-DL product under 365 nm UV light, further emphasizing the fluorescence characteristics after dialysis.

Figure S 1. *Dialysis Performance. a) Physical aspect of the first contact of the dialysis membrane with water under natural light and b,c) UV light of 365 nm.d)) Physical aspect at 72h of the dialysis membrane under natural light and g) UV light of 365 nm. h) Emission spectra of water changes and dialyzed product, i) Physical aspect of water changes and dialyzed product under UV light of 365 nm.*

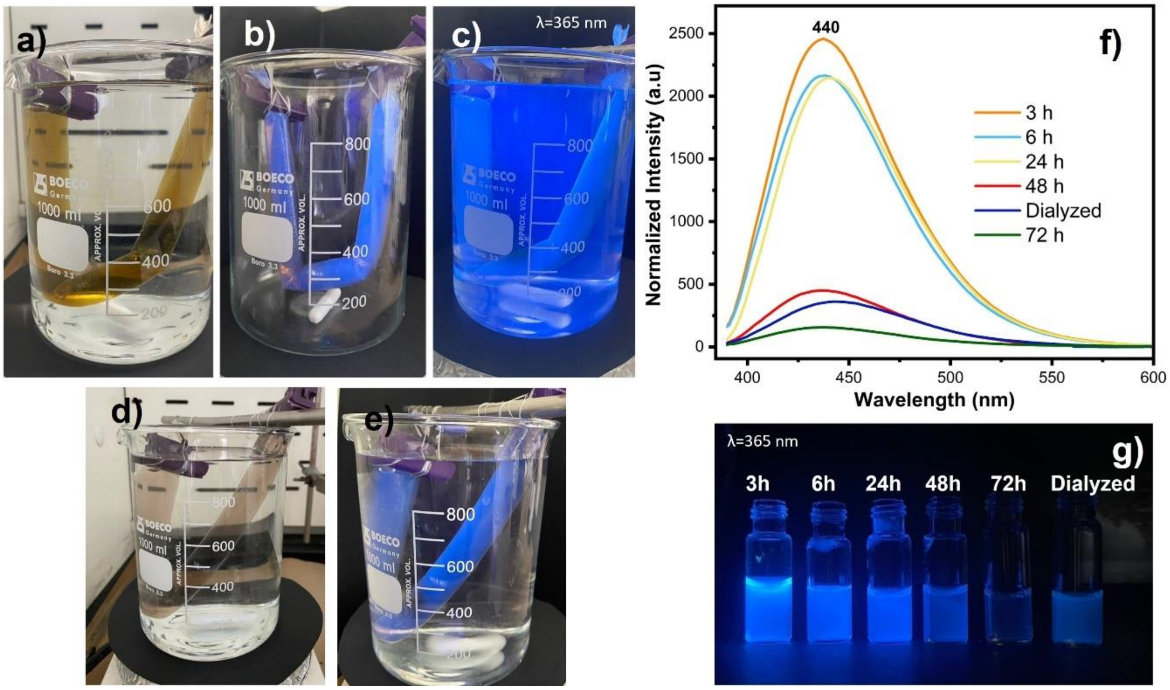

Appendix 3.Silica column performance.

Figure S 2(a), (b), and (c) illustrate the performance of the silica column purification process, beginning with the Rxn as it exits the reactor and after being dried. Following this, the column setup is depicted, highlighting the separation process. As shown in Figure S 2(e), six distinct fractions were obtained during the elution process. TLC analysis, presented in Figure S 2(f), confirmed the emissive properties of each fraction, identifying fraction 5 as the most fluorescent. This fraction was selected as the purified sample for subsequent characterization and further experimentation.

Figure S 2. *Silica columna performance. a) Rxn under natural light, b) Rxn under UV light 365 nm, c) dry Rxn, d) silica column assembly, e) fractions obtained, f) TLC of fractions obtained.*

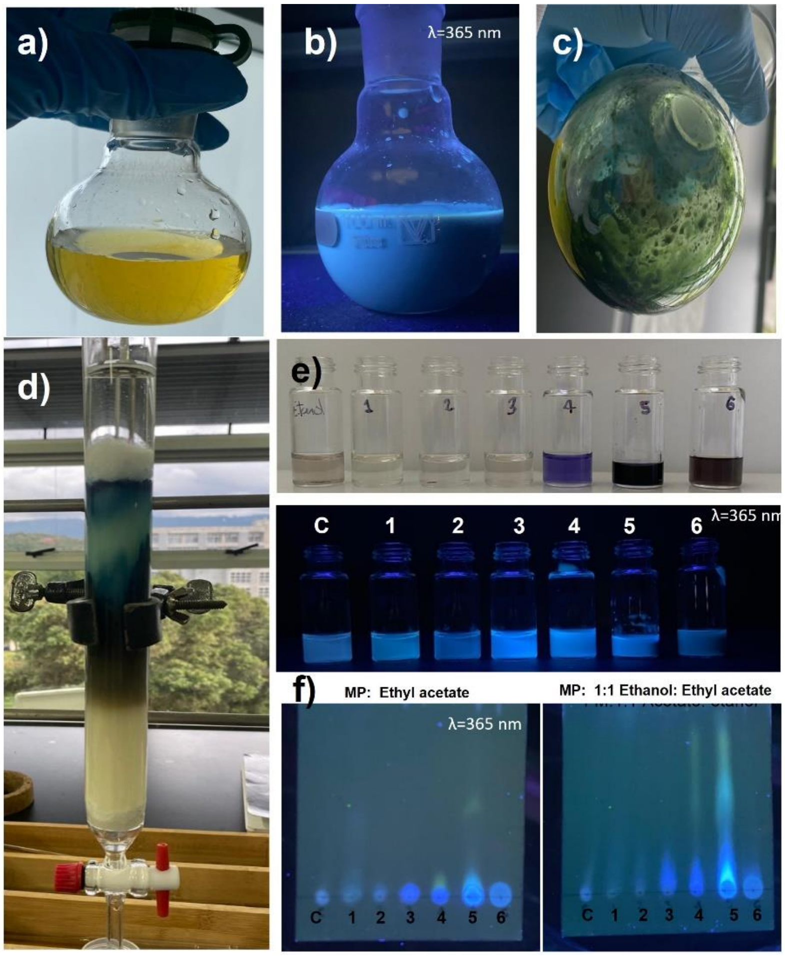

Appendix 4. Nuclear magnetic resonance (NMR) of the fraction purified by column.

The NMR spectra provide detailed insights into the structural characteristics of the purified fraction (CQDs-CC) obtained via silica column chromatography. The analysis includes the ^{1}H NMR spectrum (Figure S 3), which reveals high-field signals characteristic of saturated compounds with minimal quaternary hydrogens. The overlay of the ^{13}C and DEPT-135 spectra (Figure S 4) further elucidates the nature of the carbons present, confirming both sp^2 and sp^3 hybridizations (Wang & Hu, 2014). Finally, the HSQC spectrum (Figure S 5) highlights the interactions between carbons and hydrogens, offering a comprehensive understanding of the molecular framework of the purified fraction.

Figure S 3. *^{1}H spectrum of the purified fraction of CQDs-CC.*

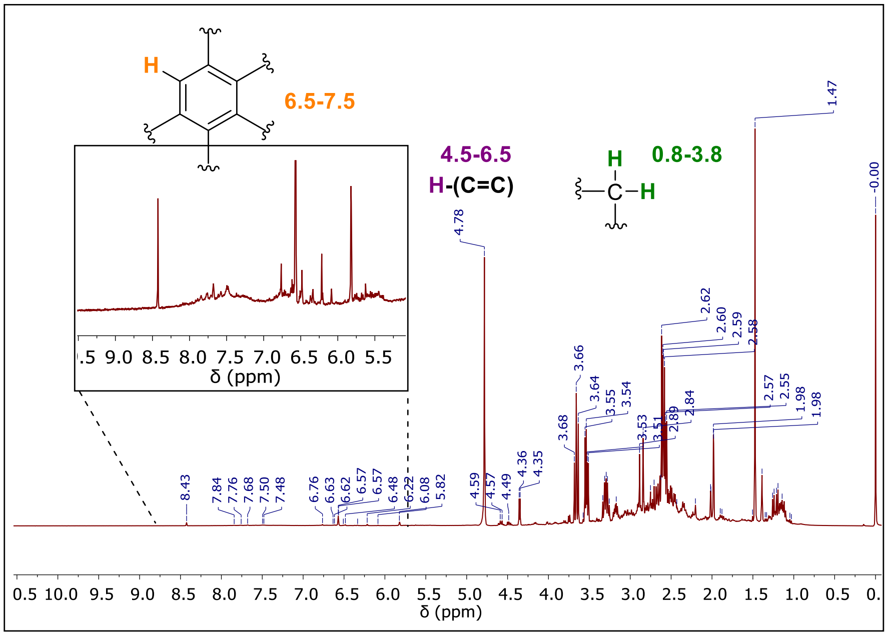

Figure S 4. *^{13}C, DEPT135 overlap spectrum of the purified fraction of CQDs-CC.*

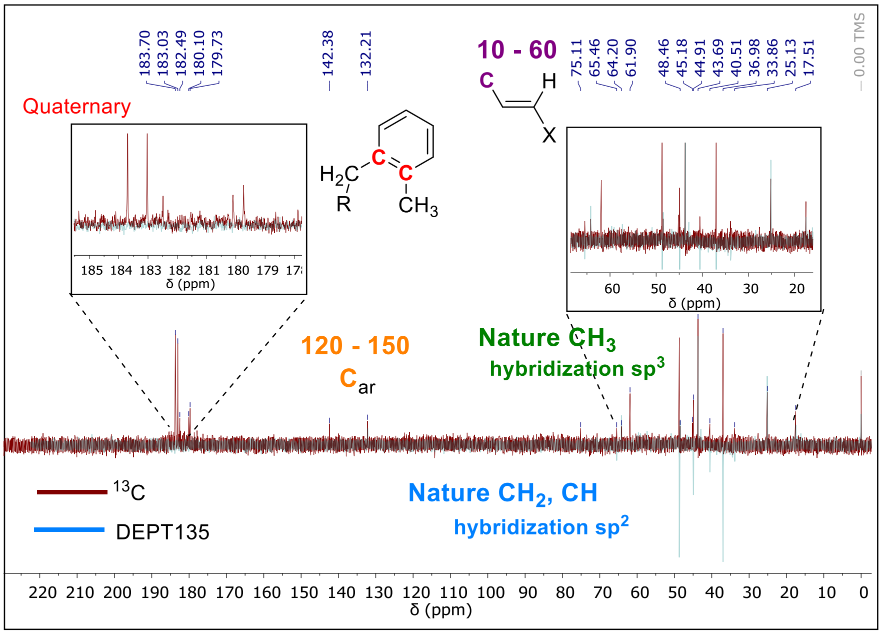

Figure S 5. *HSQC spectrum of the purified fraction of CQDs-CC.*

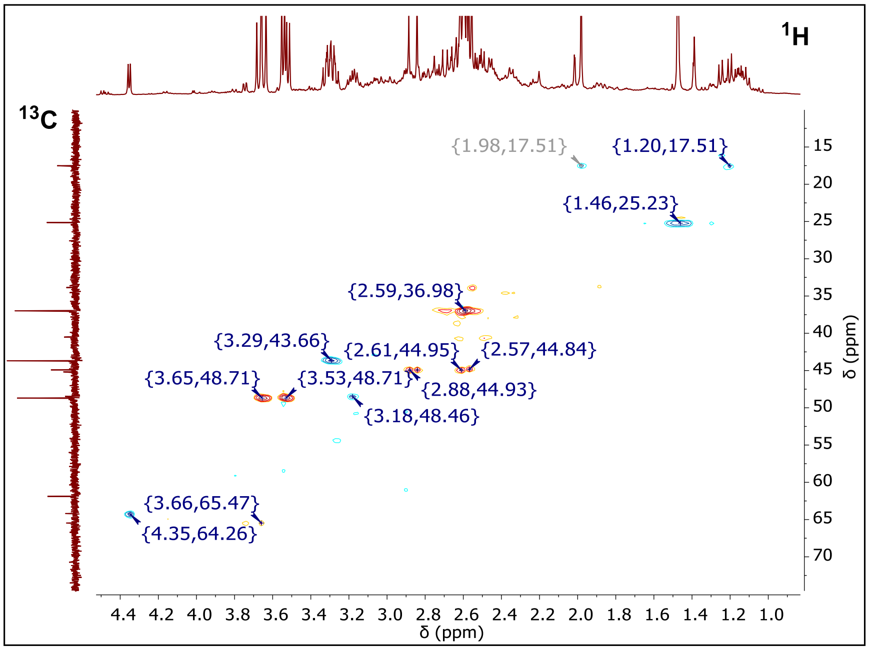

Appendix 5. Quantum yield calculation.

QY was calculated using the comparative method. Standard reference materials such as rhodamine 6G, rhodamine B, and quinine sulfate were employed as calibration standards. The consolidated QY values for the samples, calculated with reference to rhodamine 6G theoretical QY value of 0.95 (J. R. Lakowicz, 2006) are presented in Table S 2. For each standard and CQDs sample, absorbance data and the integrated emission area from the fluorescence spectra at varying concentrations were obtained. In comparative method, QY is calculated using the slope of the line determined from the plot of the absorbance against the integrated fluorescence intensities (J. R. Lakowicz, 2006). The QY was then calculated using the following equation:

$$\Phi = \Phi r . \frac{m}{m_r} \frac{n^2}{{n_r}^2}$$

Where Φ is the quantum yield, m is the slope of the line obtained from the plot of the integrated fluorescence intensity vs. absorbance. n is the refractive index of solvent, and the subscript r refers to the reference fluorophore of know QY. The results for the QY of the standards and the evaluated CQD samples are presented below, providing a comprehensive overview of their optical performance.

Table S 2. *QY obtained from the different samples.*

Muestra	**QY**
ROD 6G	0.95
ROD B	0.71
Quinine Sulfate	0.54
CQDs-CC	0.47
CQDs-DL	0.05

Figure S 6. *6G rhodamine pattern used for QY calculation.*

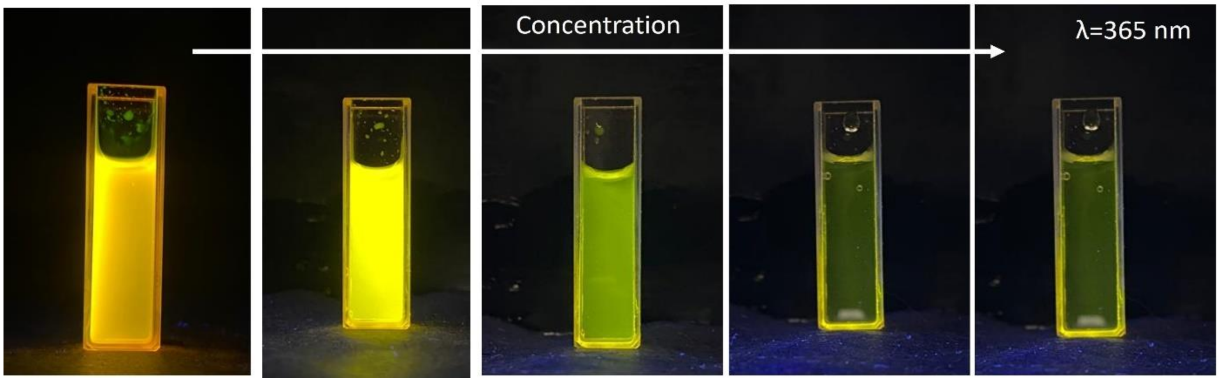

Concentration (mol/L)	Abs at 530 nm	Integrated fluorescence area
1.75x10-6	0.128	951769.363
1.35x10-6	0.098	799580.976
1x10-6	0.066	579305.589
6x10-7	0.040	365358.315
2x10-7	0.014	152618.775
0	0.000	0.000

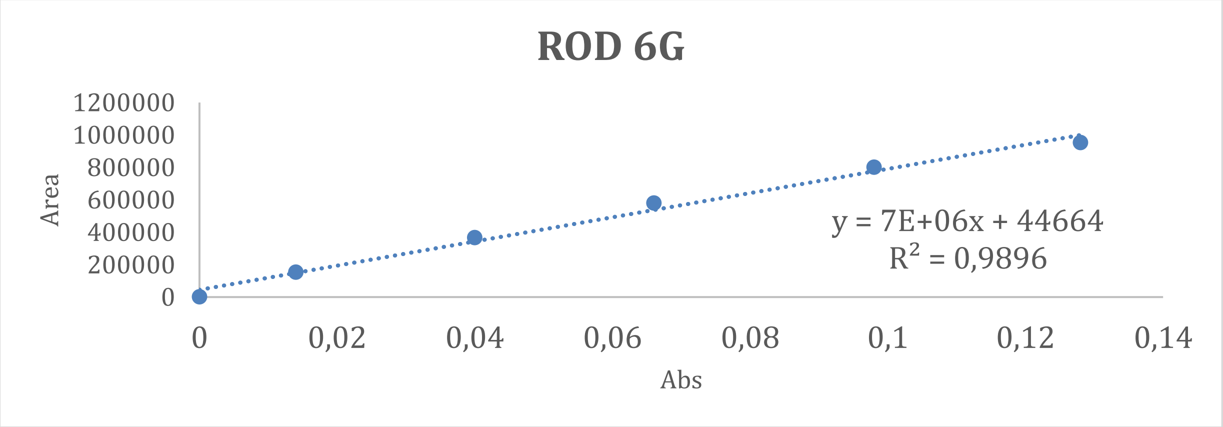

Figure S 7. *Rhodamine B pattern used for QY calculation.*

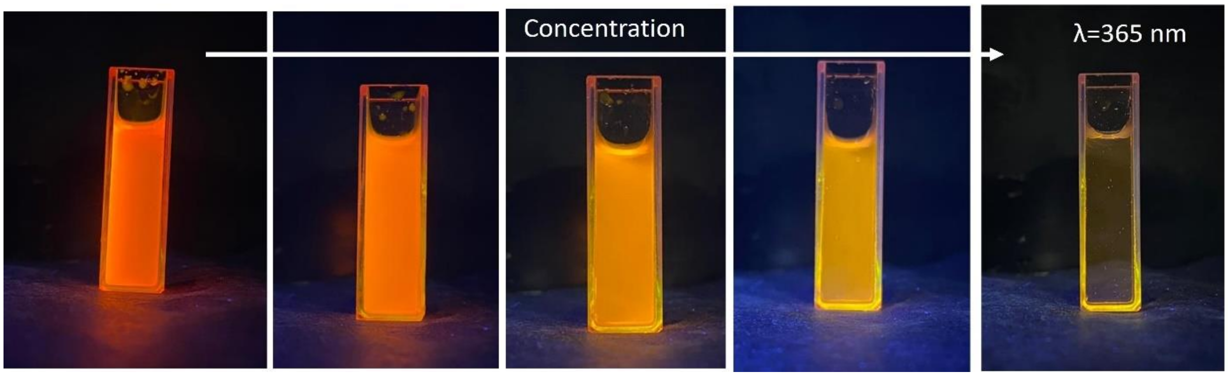

Concentration (mol/L)	Abs at 545 nm	Integrated fluorescence area
8x10-7	0.070	381182.706
6x10-7	0.052	307329.951
4x10-7	0.036	240398.194
2x10-7	0.019	123358.096
1x10-7	0.010	58412.518
0	0.000	0.000

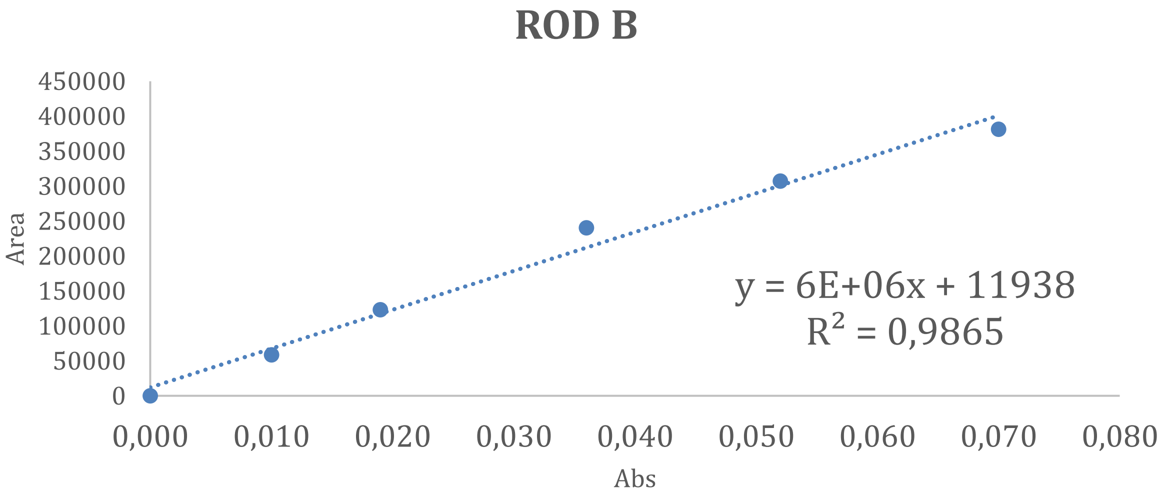

Figure S 8. Quinine sulfate pattern used for QY calculation.

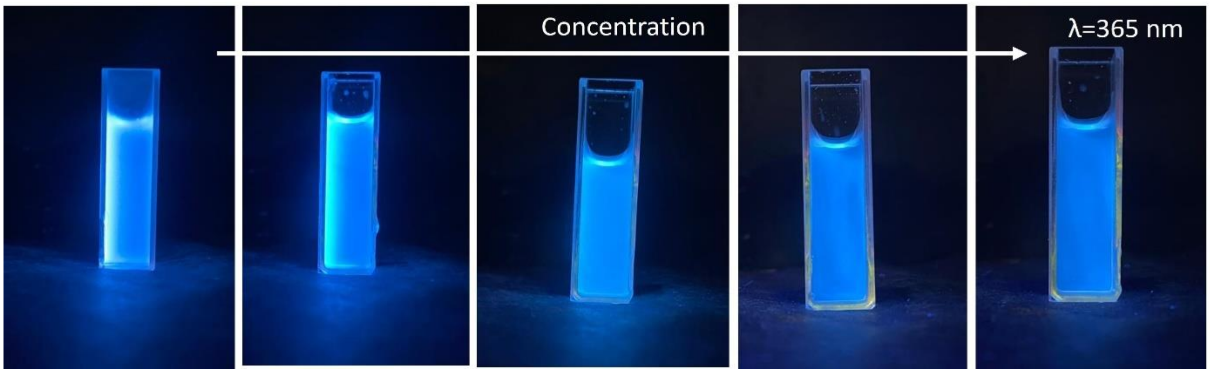

Concentration (mol/L)	Abs at 350 nm	Integrated fluorescence area
8x10-7	0.081	500873.070
6x10-7	0.053	362563.383
4x10-7	0.030	215368.739
2x10-7	0.016	152285.930
1x10-7	0.006	82786.782
0	0.000	0.000

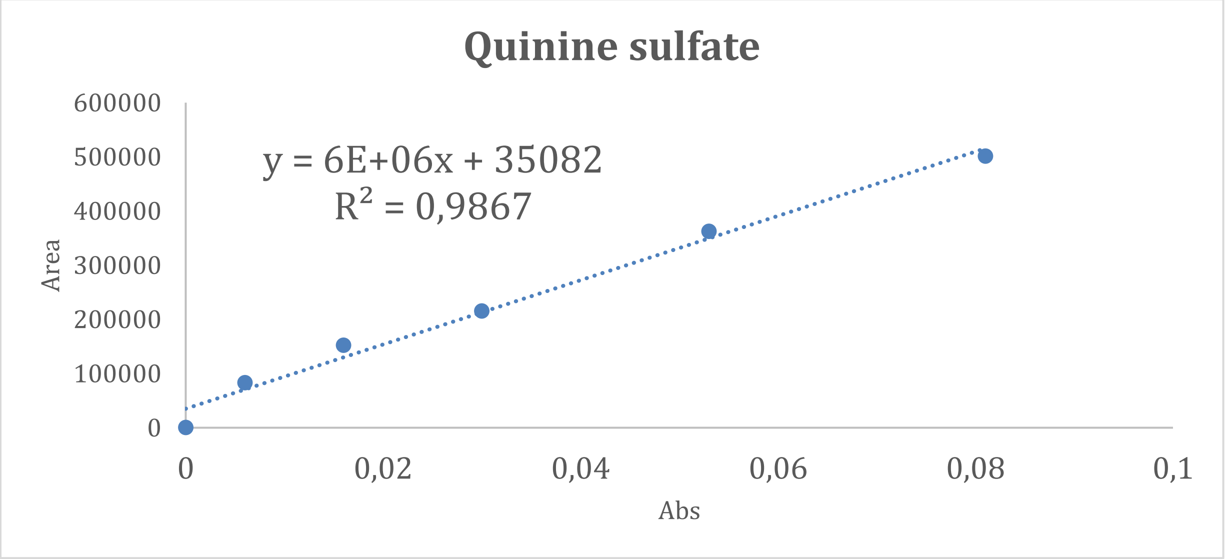

Figure S 9. *CQDs- CC used for QY calculation.*

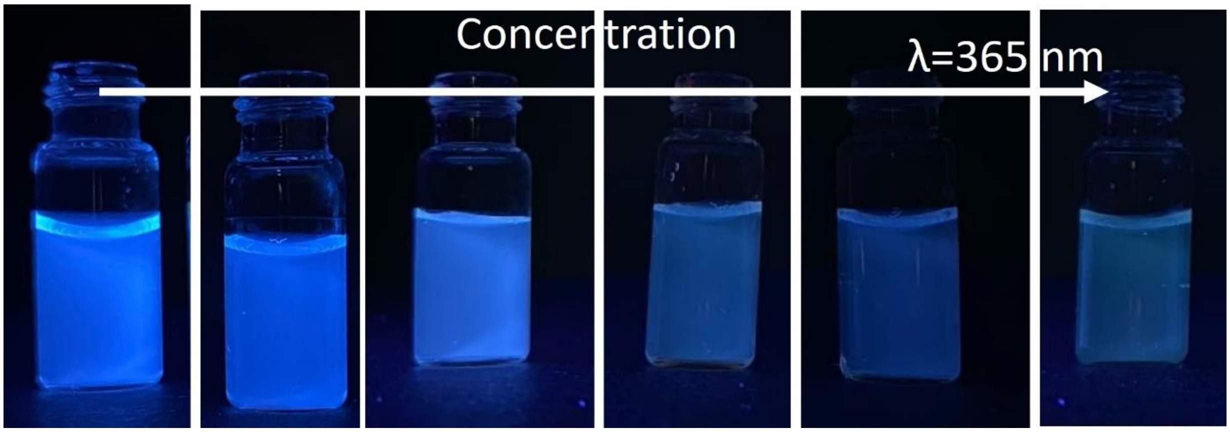

Concentration (mg/L)	Abs at 335 nm	Integrated fluorescence area
150	0.094	483468.469
100	0.057	333849.818
50	0.028	173328.122
30	0.019	109690.470
8	0.003	28913.524
0	0.000	0.000

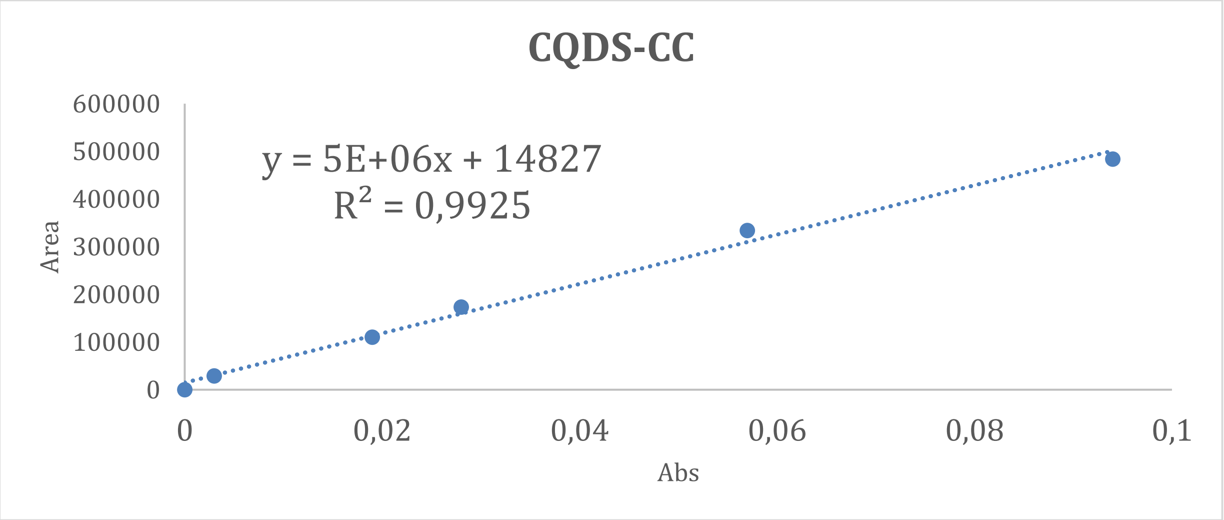

Figure S 10. *CQDs - DL used for QY calculation.*

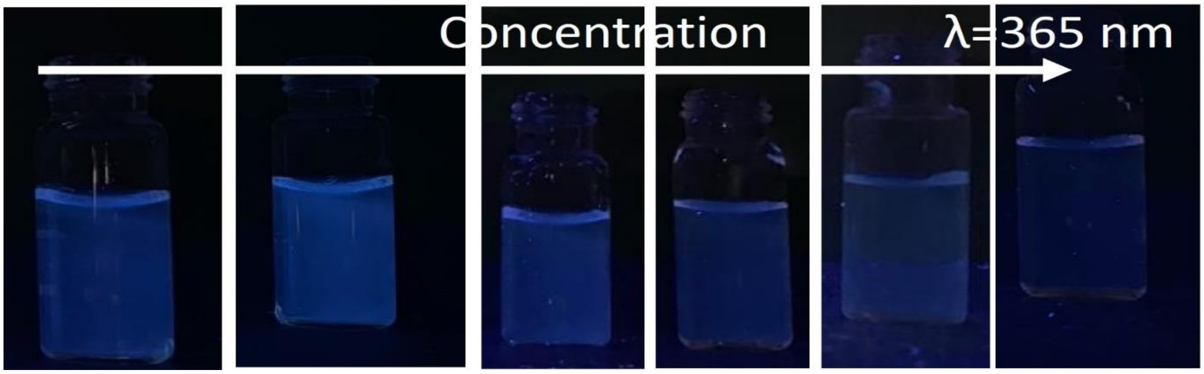

Concentration (mg/L)	Abs at 335 nm	Integrated fluorescence area
150	0.089	51618.301
100	0.074	48671.247
50	0.049	33119.876
30	0.023	15790.887
8	0.016	11049.823
0	0.000	0.000

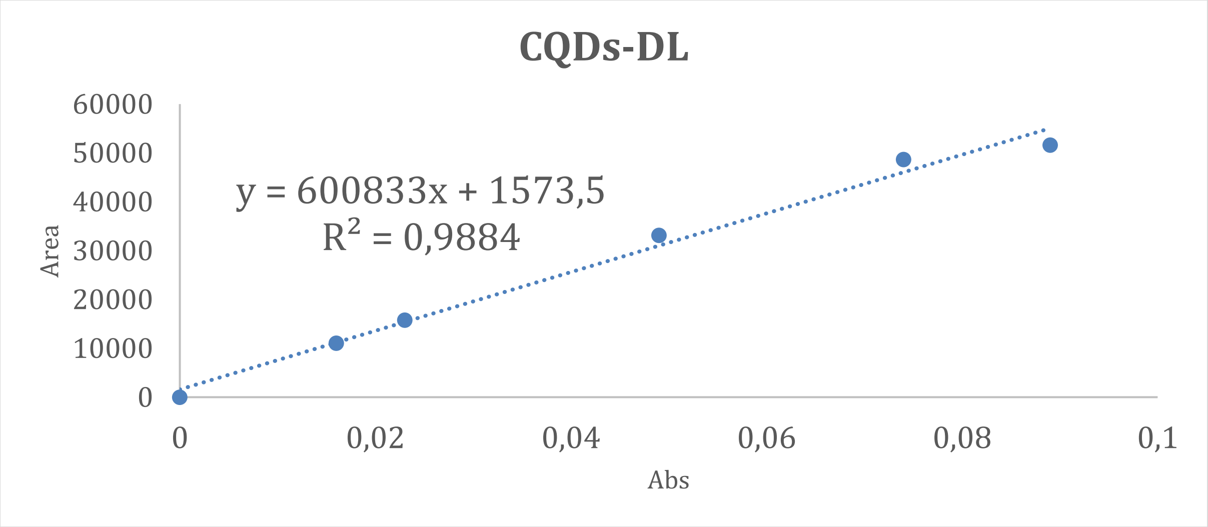

Appendix 6. ICP-OES performance.

The analysis of total mercury in natural water samples was performed using inductively coupled plasma optical emission spectrometry (ICP-OES), following the standardized methods SM 3030K and 3120B. This technique was selected due to its high sensitivity, precision, and ability to detect trace levels of mercury, making it ideal for evaluating the limits of detection (LOD) of the developed sensors. Additionally, critical parameters such as sample preparation, calibration protocols, and instrumental settings were carefully optimized to ensure accurate and reproducible results. The use of ICP-OES is particularly relevant in this context, as it provides reliable quantitative data essential for validating the sensors performance and their potential applications in environmental monitoring (Senila et al., 2014).

Table S 3. *Parameters used in the determination of ICP-OES.*

Parameter	Units	Value
Plasma gas flow	L/min	13
Auxiliary gas flow	L/min	0.2
Nebulizer gas flow	L/min	0.5
RF Power	W	1500
Pump flow rate	mL/min	1
Detection limit	mg/L	25×10^{-5}
Limit of quantification	mg/L	50×10^{-5}

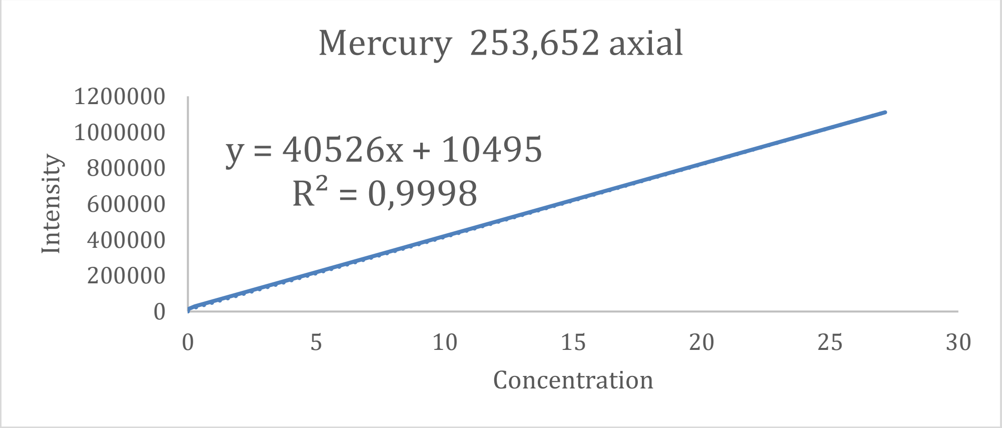

References

Akimov, Y. A. (2024). *Mie scattering theory: A review of physical features and limitations*. *4*, 1–9. https://doi.org/https://doi.org/10.48550/arXiv.2401.04146

Anpalagan, K., Yin, H., Cole, I., Zhang, T., & Lai, D. T. H. (2024). *Quantum Yield Enhancement of Carbon Quantum Dots Using Chemical-Free Precursors for Sensing Cr (VI) Ions*. *Vi*, 1–12.

Arivarasan, A., Bharathi, S., Essakinaveen, D., Arunpandiyan, S., Shanmugapriya, V., Selvakumar, B., Sasikala, G., & Jayavel, R. (2022). Investigation on the Role of antimony in CdTe QDs sensitized solar cells. *Optical Materials*, *129*(May), 112551. https://doi.org/10.1016/j.optmat.2022.112551

Bangar, S. P., & Whiteside, W. S. (2021). International Journal of Biological Macromolecules Nano-cellulose reinforced starch bio composite films- A review on green composites. *International Journal of Biological Macromolecules*, *185*(July), 849–860. https://doi.org/10.1016/j.ijbiomac.2021.07.017

Bao, H., Liu, Y., Li, H., Qi, W., & Sun, K. (2023). Luminescence of carbon quantum dots and their application in biochemistry. *Heliyon*, *9*(10). https://doi.org/10.1016/j.heliyon.2023.e20317

Calderón-Vergara, L. A., Ovalle-Serrano, S. A., Blanco-Tirado, C., & Combariza, M. Y. (2020). Influence of post-oxidation reactions on the physicochemical properties of TEMPO-oxidized cellulose nanofibers before and after amidation. *Cellulose*, *27*(3), 1273–1288. https://doi.org/10.1007/s10570-019-02849-4

Chaghaghazardi, M., Kashanian, S., Nazari, M., Omidfar, K., Joseph, Y., & Rahimi, P. (2023). Nitrogen and sulfur co-doped carbon quantum dots fluorescence quenching assay for detection of mercury (II). *Spectrochimica Acta - Part A: Molecular and Biomolecular Spectroscopy*, *293*(November 2022), 122448. https://doi.org/10.1016/j.saa.2023.122448

Chang, K., Zhu, Q., Qi, L., Guo, M., Gao, W., & Gao, Q. (2022). *Synthesis and Properties of Nitrogen-Doped Carbon Quantum*. https://doi.org/doi: 10.3390/ma15020466

Chen, C. Y., Tsai, Y. H., & Chang, C. W. (2019). Evaluation of the dialysis time required for carbon dots by HPLC and the properties of carbon dots after HPLC fractionation. *New Journal of Chemistry*, *43*(16), 6153–6159. https://doi.org/10.1039/c9nj00434c

Craig F. Bohren. (1998). *Absorption and Scattering of Light by Small Particles*. https://doi.org/https://doi.org/10.1002/9783527618156.ch5

Ding, H., Yu, S. B., Wei, J. S., & Xiong, H. M. (2016). Full-color light-emitting carbon dots with a surface-state-controlled luminescence mechanism. *ACS Nano*, *10*(1), 484–491. https://doi.org/10.1021/acsnano.5b05406

El-Shafey, A. M. (2021). Carbon dots: Discovery, structure, fluorescent properties, and applications. *Green Processing and Synthesis*, *10*(1), 134–156. https://doi.org/10.1515/gps-2021-0006

Elmizadeh, H., Soleimani, M., Faridbod, F., & Bardajee, G. R. (2019). Fabrication of a nanomaterial-based fluorescence sensor constructed from ligand capped CdTe quantum dots for ultrasensitive and rapid detection of silver ions in aqueous samples. *Spectrochimica Acta - Part A: Molecular and Biomolecular Spectroscopy*, *211*, 291–298. https://doi.org/10.1016/j.saa.2018.12.016

Escandar, G. M., & Olivieri, A. C. (2022). A Critical Review on the Development of Optical Sensors for the Determination of Heavy Metals in Water Samples. the Case of Mercury(II) Ion. *ACS Omega*, *7*(44), 39574–39585. https://doi.org/10.1021/acsomega.2c05215

García de Arquer, F. P., Talapin, D. V., Klimov, V. I., Arakawa, Y., Bayer, M., & Sargent, E. H. (2021). Semiconductor quantum dots: Technological progress and future challenges. *Science (New York, N.Y.)*, *373*(6555). https://doi.org/10.1126/science.aaz8541

Giordano, M. G., Seganti, G., Bartoli, M., & Tagliaferro, A. (2023). An Overview on Carbon Quantum Dots Optical and Chemical Features. In *Molecules* (Vol. 28, Issue 6).

https://doi.org/10.3390/molecules28062772

Gómez, F. N., Combariza, M. Y., & Blanco-Tirado, C. (2017). Facile cellulose nanofibrils amidation using a ‘one-pot’ approach. *Cellulose*, *24*(2), 717–730. https://doi.org/10.1007/s10570-016-1174-9

Guan, X., Li, Z., Geng, X., Lei, Z., Karakoti, A., Wu, T., Kumar, P., Yi, J., & Vinu, A. (2023). *Emerging Trends of Carbon-Based Quantum Dots : Nanoarchitectonics and Applications*. https://doi.org/10.1002/smll.202207181

Guo, G., & Xia, Y. (2024). General Separation of Carbon Dots by Polyamide Chromatography. *Analytical Chemistry*, *96*(13), 5095–5105. https://doi.org/10.1021/acs.analchem.3c04489

Guo, R., Li, T., & Shi, S. (2019). Aggregation-induced emission enhancement of carbon quantum dots and applications in light emitting devices. *Journal of Materials Chemistry C*, *7*(17), 5148–5154. https://doi.org/10.1039/C9TC01138B

Hama Aziz, K. H., Mustafa, F. S., Omer, K. M., Hama, S., Hamarawf, R. F., & Rahman, K. O. (2023). Heavy metal pollution in the aquatic environment: efficient and low-cost removal approaches to eliminate their toxicity: a review. *RSC Advances*, *13*(26), 17595–17610. https://doi.org/10.1039/d3ra00723e

Hinterberger, V., Damm, C., Haines, P., Guldi, D. M., & Peukert, W. (2019). Purification and structural elucidation of carbon dots by column chromatography. *Nanoscale*, *11*(17), 8464–8474. https://doi.org/10.1039/c9nr01029g

IDEAM, (Instituto de Hidrología, M. y E. A. (2021). *Protocolo de monitoreo y seguimiento del agua*. isbn: 9789585489240

IDEAM (Instituto de Hidrología, M. y E. A. (2019). *Estudio Nacional del Agua 2018*. isbn: 978-958-5489-12-7

Isogai, A., Saito, T., & Fukuzumi, H. (2011). TEMPO-oxidized cellulose nanofibers. *Nanoscale*, *3*(1), 71–85. https://doi.org/10.1039/C0NR00583E

J. R. Lakowicz. (2006). Principles of Fluorescence Spectroscopy. *Springer*, 1–4.

Jing, L., Ding, Q., Li, X., Lou, J., Liu, Z., Jiang, Y., Han, W., & Cheng, Z. (2023). Bifunctional collagen fiber/carbon quantum dot fluorescent adsorbent for efficient adsorption and detection of Pb2+. *Science of the Total Environment*, *871*(August 2022), 161989. https://doi.org/10.1016/j.scitotenv.2023.161989

Kasinathan, K., Samayanan, S., Marimuthu, K., & Yim, J. H. (2022). Green synthesis of multicolour fluorescence carbon quantum dots from sugarcane waste: Investigation of mercury (II) ion sensing, and bio-imaging applications. *Applied Surface Science*, *601*. https://doi.org/10.1016/j.apsusc.2022.154266

Kong, J., Wei, Y., Zhou, F., Shi, L., Zhao, S., Wan, M., & Zhang, X. (2024). Carbon Quantum Dots: Properties, Preparation, and Applications. In *Molecules* (Vol. 29, Issue 9). https://doi.org/10.3390/molecules29092002

Kumar, P., Dua, S., Kaur, R., Kumar, M., & Bhatt, G. (2022). A review on advancements in carbon quantum dots and their application in photovoltaics. *RSC Advances*, *12*(8), 4714–4759. https://doi.org/10.1039/D1RA08452F

Lamkin-kennard, K. A., & Popovic, M. B. (2019). 4 - Sensors: Natural and Synthetic Sensors. In *Biomechatronics*. Elsevier Inc. https://doi.org/10.1016/B978-0-12-812939-5.00004-5

Lazar, P., Mach, R., & Otyepka, M. (2019). Spectroscopic Fingerprints of Graphitic, Pyrrolic, Pyridinic, and Chemisorbed Nitrogen in N-Doped Graphene [Research-article]. *The Journal of Physical Chemistry C*, *123*, 10695–10702. https://doi.org/10.1021/acs.jpcc.9b02163

Li, H., He, X., Kang, Z., Huang, H., Liu, Y., Liu, J., Lian, S., Tsang, C. H. A., Yang, X., & Lee, S. (2010). *Water-Soluble Fluorescent Carbon Quantum Dots and Photocatalyst Design ***. 4430–4434. https://doi.org/10.1002/anie.200906154

Lv, H., Wang, S., Wang, Z., Meng, W., Han, X., & Pu, J. (2022). Fluorescent cellulose-based hydrogel with carboxymethyl cellulose and carbon quantum dots for information storage and fluorescent anti-counterfeiting. *Cellulose*, *29*(11), 6193–6204.

https://doi.org/10.1007/s10570-022-04643-1

Ma, H., Cheng, Z., Li, X., Li, B., & Fu, Y. (2023). *Advances and challenges of cellulose functional materials in sensors*. *8*(November 2022), 15–32. https://doi.org/10.1016/j.jobab.2022.11.001

Malik, S., Muhammad, K., & Waheed, Y. (2023). Nanotechnology: A Revolution in Modern Industry. *Molecules*, *28*(2). https://doi.org/10.3390/molecules28020661

Mansuriya, B. D., & Altintas, Z. (2021). Carbon dots: Classification, properties, synthesis, characterization, and applications in health care-an updated review (2018–2021). *Nanomaterials*, *11*(10). https://doi.org/10.3390/nano11102525

Martínez-Ramírez, A. P., Rincón-Ortiz, S. A., Baldovino-Medrano, V. G., Blanco-Tirado, C., & Combariza, M. Y. (2023). Influence of reaction variables on the surface chemistry of cellulose nanofibers derived from palm oil empty fruit bunches. *RSC Advances*, *13*(51), 36117–36129. https://doi.org/10.1039/D3RA06933H

Meng, W., Bai, X., Wang, B., Liu, Z., Lu, S., & Yang, B. (2019). Biomass-Derived Carbon Dots and Their Applications. *Energy and Environmental Materials*, *2*(3), 172–192. https://doi.org/10.1002/eem2.12038

Mintz, K. J., Zhou, Y., & Leblanc, R. M. (2019). Recent development of carbon quantum dots regarding their optical properties, photoluminescence mechanism, and core structure. *Nanoscale*, *11*(11), 4634–4652. https://doi.org/10.1039/C8NR10059D

Mudasir, M., Baskara, R. A., Suratman, A., Yunita, K. S., Perdana, R., & Puspitasari, W. (2020). Simultaneous Adsorption of Zn(II) and Hg(II) Ions on Selective Adsorbent of Dithizone-Immobilized Bentonite in the Presence of Mg(II) Ion. *Journal of Environmental Chemical Engineering*, *8*(4), 104002. https://doi.org/10.1016/j.jece.2020.104002

Munson, C. A., Gottfried, J. L., De Lucia, F. C., McNesby, K. L., & Miziolek, A. W. (2007). Laser-based detection methods of explosives. In *Counterterrorist Detection Techniques of Explosives*. Elsevier B.V. https://doi.org/10.1016/B978-044452204-7/50029-8

Noun, F., Jury, E. A., & Naccache, R. (2021). *Elucidating the Quenching Mechanism in Carbon*

Dot-Metal Interactions – Designing Sensitive and Selective Optical Probes. 1–13. https://doi.org/https://doi.org/10.3390/s21041391

Ozyurt, D., Kobaisi, M. Al, Hocking, R. K., & Fox, B. (2023). Properties, synthesis, and applications of carbon dots: A review. *Carbon Trends*, *12*(June), 100276. https://doi.org/10.1016/j.cartre.2023.100276

Padilla-vaca, F., Mendoza-macías, C. L., Franco, B., Anaya-velázquez, F., Ponce-noyola, P., & Flores-martínez, A. (2018). *El mundo micro en el mundo nano : importancia y desarrollo de nanomateriales para el combate de las enfermedades causadas por bacterias , protozoarios y hongos The micro world in the nano world : Importance and development of nanomaterials for the fight a*. *11*(21), 15–28. https://doi.org/https://doi.org/10.22201/ceiich.24485691e.2018.21.62591

Reshmy, R., Philip, E., Thomas, D., Madhavan, A., Sindhu, R., & Binod, P. (2021). Bacterial nanocellulose: engineering, production, and applications. *Bioengineered*, *12*(2), 11463–11483. https://doi.org/10.1080/21655979.2021.2009753

Rodríguez, C. (2019). *Evaluación de la calidad del agua del río Vetas relacionada con la minería urífera practicada en la provincia de Soto en Santander* (p. 26). https://ridum.umanizales.edu.co/xmlui/bitstream/handle/20.500.12746/3413/documento maestria FINAL 18 MAYO (2).pdf?sequence=1

Saavedra-Sanabria, O. L., Durán, D., Cabezas, J., Hernández, I., Blanco-Tirado, C., & Combariza, M. Y. (2021). Cellulose biosynthesis using simple sugars available in residual cacao mucilage exudate. *Carbohydrate Polymers*, *274*(April), 1–12. https://doi.org/10.1016/j.carbpol.2021.118645

Senila, M., Drolc, A., Pintar, A., Senila, L., & Levei, E. (2014). Validation and measurement uncertainty evaluation of the ICP-OES method for the multi-elemental determination of essential and nonessential elements from medicinal plants and their aqueous extracts. *Journal of Analytical Science and Technology*, *5*(1), 37. https://doi.org/10.1186/s40543-014-0037-y

Sharma, A., Thakur, M., Bhattacharya, M., Mandal, T., & Goswami, S. (2019). Commercial application of cellulose nano-composites – A review. *Biotechnology Reports*, *21*, e00316. https://doi.org/10.1016/j.btre.2019.e00316

Sharma, G., Tara, A., & Sharma, V. D. (2017). *Advances in monolithic silica columns for high-performance liquid chromatography*. https://doi.org/10.1186/s40543-017-0125-x

Singh, S. S., Salem, D. R., & Sani, R. K. (2021). Spectroscopy, microscopy, and other techniques for characterization of bacterial nanocellulose and comparison with plant-derived nanocellulose. In *Microbial and Natural Macromolecules* (pp. 419–454). Elsevier. https://doi.org/10.1016/b978-0-12-820084-1.00018-1

Subbotina, E., Montanari, C., & Berglund, L. (2022). *composites with both sustainable production and fiber recycling systems †. 1*, 570–576. https://doi.org/10.1039/d1ta07758a

Sufficiency, E., Qamar, S. A., Ferreira, L. F. R., Franco, M., Iqbal, H. M. N., & Bilal, M. (2022). Emerging biotechnological strategies for food waste management: A green leap towards achieving high-value products and environmental abatement. *Energy Nexus*, *6*, 100077. https://doi.org/https://doi.org/10.1016/j.nexus.2022.100077

Tan, Q., Li, X., Wang, L., Zhao, J., Yang, Q., Sun, P., Deng, Y., & Shen, G. (2022). One-step synthesis of highly fluorescent carbon dots as fluorescence sensors for the parallel detection of cadmium and mercury ions. *Frontiers in Chemistry*, *10*(September), 1–14. https://doi.org/10.3389/fchem.2022.1005231

United Nations Environment Programme (UNEP). (2013). *Mercury: time to act* (1st ed.). isbn: 9789280733105

Vonnie, J. M., Ting, B. J., Rovina, K., Aqilah, N. M. N., Yin, K. W., & Huda, N. (2022). Natural and Engineered Nanomaterials for the Identification of Heavy Metal Ions—A Review. *Nanomaterials*, *12*(15). https://doi.org/10.3390/nano12152665

Wang, Y., & Hu, A. (2014). *Carbon quantum dots : synthesis , properties and applications*. 6921–6939. https://doi.org/10.1039/c4tc00988f

Xu, X., Ray, R., Gu, Y., Ploehn, H. J., Gearheart, L., Raker, K., & Scrivens, W. A. (2004).

Electrophoretic analysis and purification of fluorescent single-walled carbon nanotube fragments. *Journal of the American Chemical Society*, *126*(40), 12736–12737. https://doi.org/10.1021/ja040082h

Xue, B., Yang, Y., Tang, R., Sun, Y., & Sun, S. (2019). One-step hydrothermal synthesis of a flexible nanopaper- based Fe 3 + sensor using carbon quantum dot grafted cellulose nanofibrils. *Cellulose*, *7*. https://doi.org/10.1007/s10570-019-02846-7

Yadav, P. K., Chandra, S., Kumar, V., Kumar, D., & Hasan, S. H. (2023). Carbon Quantum Dots: Synthesis, Structure, Properties, and Catalytic Applications for Organic Synthesis. In *Catalysts* (Vol. 13, Issue 2). https://doi.org/10.3390/catal13020422

Yi, H., Liu, J., Yao, J., Wang, R., Shi, W., & Lu, C. (2022). Photoluminescence Mechanism of Carbon Dots: Triggering Multiple Color Emissions through Controlling the Degree of Protonation. *Molecules*, *27*(19). https://doi.org/10.3390/molecules27196517

Zhang, P., Yang, M., Lan, J., Huang, Y., Zhang, J., Huang, S., Yang, Y., & Ru, J. (2023). Water Quality Degradation Due to Heavy Metal Contamination: Health Impacts and Eco-Friendly Approaches for Heavy Metal Remediation. *Toxics*, *11*(10). https://doi.org/10.3390/toxics11100828

Zheng, J., Xie, Y., Wei, Y., Yang, Y., & Liu, X. (2020). *An Efficient Synthesis and Photoelectric Properties of Green Carbon Quantum Dots with High Fluorescent Quantum Yield*. 1–15.

Zhu, H., Huang, X., Deng, Y., Chen, H., Fan, M., & Gong, Z. (2023). Applications of nanomaterial-based chemiluminescence sensors in environmental analysis. *TrAC - Trends in Analytical Chemistry*, *158*, 116879. https://doi.org/10.1016/j.trac.2022.116879

Zou, W., Ma, X., & Zheng, P. (2020). Preparation and functional study of cellulose/carbon quantum dot composites. *Cellulose*, *27*(4), 2099–2113. https://doi.org/10.1007/s10570-019-02926-8